Vaasan yliopisto
UNIVERSITY OF VAASA

REINO VIRRANKOSKI
(Ed.)

Wireless Sensor Systems in Indoor Situation Modeling II (WISM II)

PROCEEDINGS OF THE UNIVERSITY OF VAASA
REPORTS 188


Aalto University
School of Electrical
Engineering


Vaasan yliopisto
UNIVERSITY OF VAASA


VTT

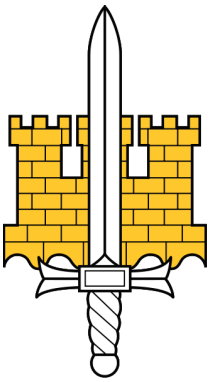


TEKES

PREFACE

This is the final report of the project *Wireless Sensor Systems in Indoor Situation Modeling II* (WISM II). The project took place on 11/2010-02/2013. It was funded by participating companies and research organizations, by Finnish Defence Forces and by the Safety and Security program of the Finnish Funding Agency for Technology and Innovation (Tekes). Participating research organizations were Department of Automation and Systems Technology and Department of Communications and Networking in Aalto University, Communications and Systems Engineering Group of the Department of Computer Science in the University of Vaasa, Department of Military Technology in Finnish National Defence University and VTT Technical Research Centre of Finland.

AUTHORS

Mikael Björkbom	Aalto University
Huseyin Yigitler (Yusein Ali)	Aalto University
Ossi Kaltiokallio	Aalto University
Maurizio Bocca	Aalto University, University of Utah
Matthieu Myrsky	Aalto University
Marek Matusiak	Aalto University
José Vallet	Aalto University
Jari Saarinen	Aalto University
Riku Jäntti	Aalto University
Heikki Koivo	Aalto University
Caner Çuhac	University of Vaasa
Tobias Glocker	University of Vaasa
Reino Virrankoski	University of Vaasa
Mohammed Elmusrati	University of Vaasa
Jussi Timonen	National Defence University
Jouko Vankka	National Defence University
Hannu H. Kari	National Defence University
Marko Korkalainen	VTT
Mikko Lindholm	VTT
Heikki Ailisto	VTT

Contents

1 INTRODUCTION

Situation awareness plays a key role in modern safety, security, rescue and military operations. The more complete picture one has about an ongoing situation, the better he can plan and execute his operation. Since the situation which requires involvement by safety, security, rescue or military forces is typically highly dynamic with many rapid changes, the situation model must also be dynamic and update the observed changes as real-time as possible. The presentation of the situation model must be detailed but simultaneously easy to understand, which sets challenges to the usability design.

Building interior provides especially challenging environment for the situation modeling, because many important monitoring and localization systems, such as satellites, areal radars and airplanes (including RC planes and UAVs) cannot be used to monitor building interior from outside. Wireless sensor and actuator networks consisting of sensor platforms equipped with several sensors capable to form a wireless network can be utilized to collect measurements from the building interior to form a situation model. Some of the actuators can be mobile and enter to the building. The mobile ones can carry static (non-mobile) sensor nodes and deploy them on their route. Alternatively, the static nodes can be shot into the building by using carrier grenades. The friendly forces (police, rescue, soldiers, etc.) entering to the building can be equipped with wearable sensor system, which will monitor the environment, assist indoor navigation and provide information about the activities of the group and its individual members inside the building during the action.

In this WISM II project we developed new algorithms for device free localization, for indoor navigation, for indoor space mapping, for image processing in sensor nodes, for data management and for the computation, visualization and distribution of the common operational picture (COP). By utilizing these algorithms we made a fully integrated wireless sensor system, which produces a real-time situation model of the building interior. Static nodes can be deployed to the building by using a mobile robot, which is part of the system. After the preliminary tests of the subsystems, the integrated system was tested and demonstrated at the urban warfare training site (so-called Helsinki Simulator) at Finnish National Defence University in Santahamina [1].

The project duration was 1.11.2010–28.2.2013. It was funded by Finnish Funding Agency for Technology and Innovation's program Safety and Security 2007–2013 (Tekes Turvallisuus 2007–2013), by six participating companies, by three participating research organizations and by Finnish Defence Forces. Finnish Po-

lice participated such that they provided information about the operational needs and requirements in their point of view. From the police side the participating unit was originally Police Operative Unit in the Finnish Ministry of the Interior and, after the changes in the police administration, Police Academy. System tactical and operative requirements were defined by National Defence University and by Police.

2 CURRENT STATE OF THE ART

2.1 Background

Wireless sensor systems have been developing rapidly since the beginning of 2000's. Many of the early ideas to form ad hoc networks by using miniaturized devices called sensor nodes were rising from the development of the military monitoring and communication systems. Since then, the development of the wireless sensor and actuator networks has also spread into many other important application areas, such as wireless automation [2].

In general, wireless sensor nodes are devices equipped with radio, one or several sensors, microcontroller (or microprocessor) and some memory and power source. There are two conflicting main interests in the sensor node development; on the one hand the node size and energy consumption must be minimized, but on the other hand the node must achieve as good performance (sample rate, data transfer capability, computation power) as possible with its scarce resources. The wireless sensor network (WSN) consisting of wireless sensor nodes can operate without fixed base stations or fixed number of nodes. The nodes can communicate directly with each other by using either direct radio link or a multi-hop path, which consist of several radio links between the nodes. To enable this, the networking protocols must operate in a distributed manner. Distributed networking allows distributed computation such that a remarkable amount of data can be processed in a network in a fully distributed or locally centralized manner, and only the requested information will be submitted trough the gateway from the WSN to the upper levels of the communication system.

Once the WSN technology has developed from its early levels, it has also diverged. Some developers put their main focus on the minimization of node size and energy consumption. These nodes are often used for such applications, where the main purpose of the wireless network is to collect measurements which are then analyzed in a centralized manner outside the wireless network. Some developers emphasize also the idea of distributed network operation, which requires distributed algorithms and nodes with more resources. Node size and energy consumption are then compromises between the minimization and performance requirements. However, since the microprocessors, power sources and other electronic components are still developing rapidly, it is probable to achieve higher performance with smaller device size and lower energy consumption in the nearby future.

2.2 Wireless Sensor Networks in Situational Awareness

Wireless sensor network can be utilized to collect several types of measurements from the battlefield. More complete operational picture can then be computed by combining the sensor measurements with other sources of information by advanced data fusion. Since the sensor nodes are much smaller and cheaper that many other monitoring devices, many of them can be deployed to the battlefield to get more complete and redundant data. The distributed nature makes it also more difficult to cripple or destroy the network, because the loss of some sensor nodes does not block the network operation.

Sensor node deployment and localization is easier outside, because then the nodes can be scattered from the air and they can utilize satellite positioning in their localization. Neither of these is possible inside a building. There the nodes must be deployed by using mobile devices which can carry and deploy the static (non-mobile) nodes or by using carrier grenades to shoot the nodes inside. Once the friendly forces enter to the building they can also carry sensor nodes with them and deploy them on their route. Localization must be based on distance estimation between the nodes, which is challenging to do by using only the radio signal. Also the radio environment is more difficult inside the building, because there is no similar line of sight conditions as there can be outside, and there can be many kinds of structures which can block the radio signal.

There exists a huge amount of industrial sensors that can be used in the sensor nodes. Some of the sensors, which are important for situational awareness, are microphones, miniaturized cameras, passive infrared sensors, accelerometers, air pressure sensors, light intensity sensors and temperature and humidity sensors. These ones are usually also relatively cheap. More specialized sensors, such as so-called e-noses to develop poisonous chemicals or explosives, have also been developed, but they are more expensive and more complicated to implement and operate.

In general, energy efficiency and energy resources are very critical issues in the development of wireless sensor networks, but in the context of indoor situational awareness these requirements are somehow easier. In industrial automation the system lifetime should be several years, but in the case of police, military or rescue operation inside a building the operation time is typically at most a couple of hours, and it can be even shorter. Thus, more sensor node energy resources can be sacrificed in a short time to be able to compute as complete and as real time situation model as possible. On the other hand, communication reliability and security, localization accuracy and data transmission capability are important.

3 OPERATIONAL REQUIREMENTS

3.1 General

Urban situation awareness and especially localization information is important in many applications. Operations, such as search-and-rescue, military operations, urban combat, hostage situations, emergency situations, indoor fire, or earthquake damaged buildings, rely on localization information, as the map and location of targets in possibly unknown area is needed. Combining information from several subsystems is a key aspect in these perilous applications. Knowing where things are and combining several sources of information, enables one to make context aware data gathering, analysis and decisions, in short situation awareness. In Chapter 4, we present the developed solution for indoor situation awareness. It is an integrated system that provides localization services of several types to enable situation awareness with focus on an urban environment. Multiple localization services are provided in a common frame of reference, as well as visualization of other sensor data. The information and common operational picture of the system is conveyed to all parties involved in the operation, field team and people in the command post [1, 3, 4].

3.2 Pre-surveillance

Pre-surveillance is performed before sending any troops to the action. Its purpose is to gather as much information as possible about the situation inside the building and its immediate surrounding environment as fast as possible. This information is then used as a basis for the operation planning before taking the action. There are certain priorities in the information that should be extracted. The most important thing to know is the location of the people inside the building and an exact number or estimate of how many of them are there. Second important thing is to perform mapping inside the building if its structure (rooms, corridors, doors etc.) is not known in advance. As a third thing, we want to figure out which one of the people inside are friendly (or neutral) and which one are enemies. After finding out these things the next task is to follow what the people are doing in the building. The actions of the enemies as well as information about that if there is somebody who seems to be injured are both important. In some special operations we may also want to know if some person who is already listed in police or intelligence databases is present. For example, a face or speaker identification can be used to match the collected samples against the ones in the database.

System unnoticeability is important during the pre-surveillance. If the enemy detects that it is monitored, it will try to disable the monitoring system and it starts to prepare to defend itself from the attack. Because of the small size of the sensor nodes and the possibility to scatter many of them, wireless sensor network fits well to pre-surveillance, but its deployment inside a building is a challenge. One option is to use autonomous mobile robot that carries and deploys the sensor nodes, as we did in this project [1]. There can be also other options, such as nodes which are capable to fly or carrier grenades to shoot the nodes in.

The operation plan must update continuously during the pre-surveillance, because it is all the time possible that something fatal happens that requires immediate action. These kinds of happenings can be, for example, shooting inside the building or sudden rapid change in a way how the building burns in fire rescue operation.

3.3 Action

Once the own troops enter to the building, it is important to provide them a common operational picture (COP), which is updated in real time. In practice real time means as real time as possible. Information about the location and movement of other people inside the building is important as well as the navigation and recognition of friendly forces. The system can help the entering troops to differentiate between enemies and hostages or other civilians. It can also inform the troops if there are new enemy intruders detected. The sensor nodes which are deployed during the pre-surveillance phase can form a joint network with the ones carried by the friendly forces. These networks can collaboratively produce more information to computer the COP, and also assist each other in indoor navigation. In addition to sharing the COP among the troops operating in the building and its immediate surroundings, it can also be transmitted to the upper levels of the command chain. This requires a long distance link and interfacing to connect the local area networks used in the indoor situation modeling with the rest of the tactical communication system.

One thing to notice is that typically the period the action takes is short, from some minutes to some hours. Thus, the usual energy constrains which must be taken into account in WSN design are not as strict as they are in some other applications, such as industrial automation. In indoor situation modeling more resources can be sacrificed during the action to be able to compute as accurate and real-time updating situation model as possible for the own troops which are taking the action inside the building.

4 DEVELOPED ARCHITECTURE

4.1 System Concept

The indoor situation modeling system we developed consist of the following subentities: deployable WSN, mobile robot, wearable sensor system, IceStorm middleware for data management, COP server for common operational picture computation, visualization and distribution, and PDAs for COP presentation. Each one of the monitoring systems can operate without the other ones, but once they are all used, the situation model becomes more complete. The subsystems can also assist each other, for example, in sensor node deployment and in localization computation [1].

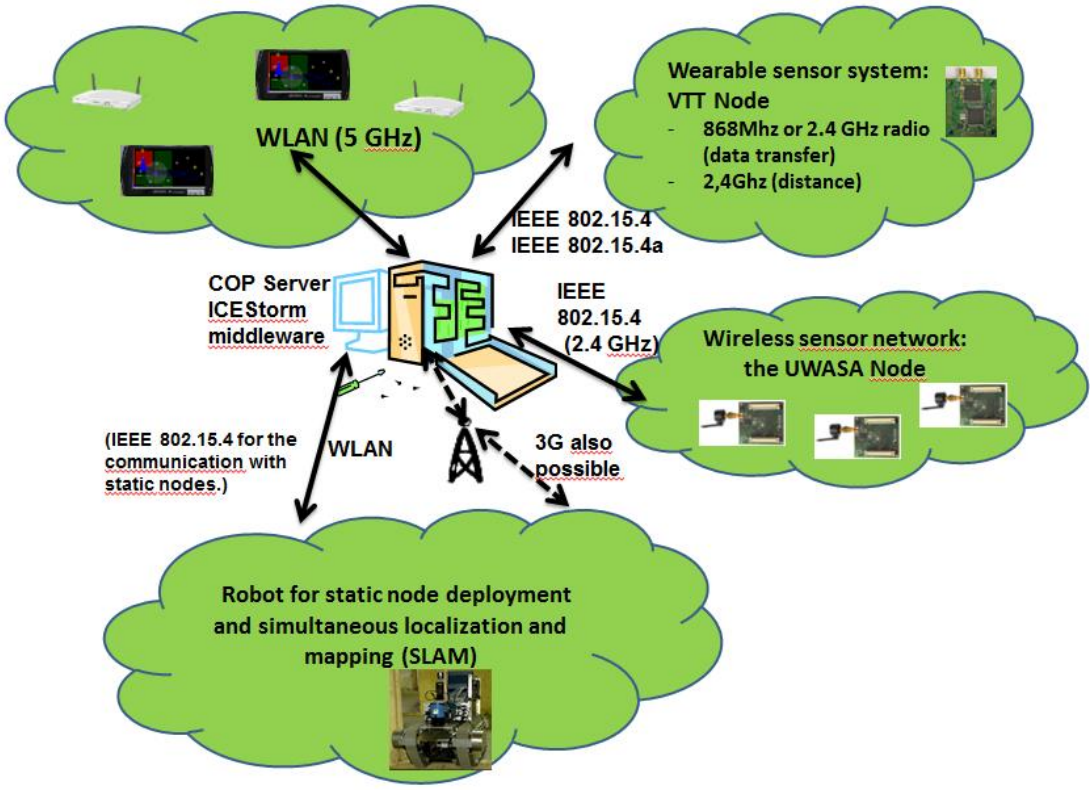

Figure 4.1.1. Developed indoor situation modeling system architecture.

IceStorm middleware is used to collect and log down the data from different subsystems. COP server then orders the data it needs for COP computation by using IceStorm. In addition to WNS and robot sensor measurements, this software architecture allows us to add also other sources of information to COP, if such

sources are available. In our demonstration we stacked the situation in the building and its immediate surrounding on top of Esri's maps.

We applied IEEE 802.15.4 and IEEE 802.15.4a communication protocols in 2.4 GHz and 868 MHz frequency bands in sensor networks. IEEE 802.11 was used in mobile robot communication and in the communication of the portable devices carried by the friendly forces. The frequency bands for the robot and PDAs were 2.4 GHz and 5 GHz respectively. All these networks formed one system and operated simultaneously (see the following subchapters for further details). One reason to use also 5 GHz WLAN was to avoid channel overlapping with the robot communication and the sensor network

4.2 Mobile Robot

A mobile robot provides many benefits in emergency situation; most importantly, it can be deployed to gather information about an unknown situation without risking human lives. In the demonstrated indoor situation modeling system, the robot is in central role in creating a common frame of reference for the system. In this study a remote-controlled robot is used as a scout. The robot builds a metric map of the environment while exploring, and localizes itself against the same map. In addition, the robot deploys static nodes into known locations in the environment. The robots position along with the RSS measurements recorded along the trajectory are used to localize the unknown nodes.

The mobile robot system is illustrated in Figure 4.2.1. The robot is a tracked platform, weighting approximately 100 kg and carries along 100 Ah of energy as well as sensors and computation power. Further details about the robotic system can be found from [5]. In this article we use a laser range finder (SICK LMS 111) and dead reckoning for creating the map and a camera with pan-tilt-unit for providing feedback for the operator. In addition, the robot is equipped with a communication subsystem which enables the communication with the robot practically in all environments without a need for site-specific infrastructures.

Finally, the robot has a wireless sensor node distribution system installed inside of it. An operator can deploy the wireless sensors into strategic places in the building. The deployed nodes are location labeled to the position that the robot dropped them.

Figure 4.2.1. The mobile robot used as a part of WISM II system architecture.

The robot is controlled by means of teleoperation from a command center. The laser range finder data, the image from the camera, the calculated position and the constructed map of the area (see section 5.2.1) are sent to the operator. The visualization of the data is shown in Figure 4.2.2.

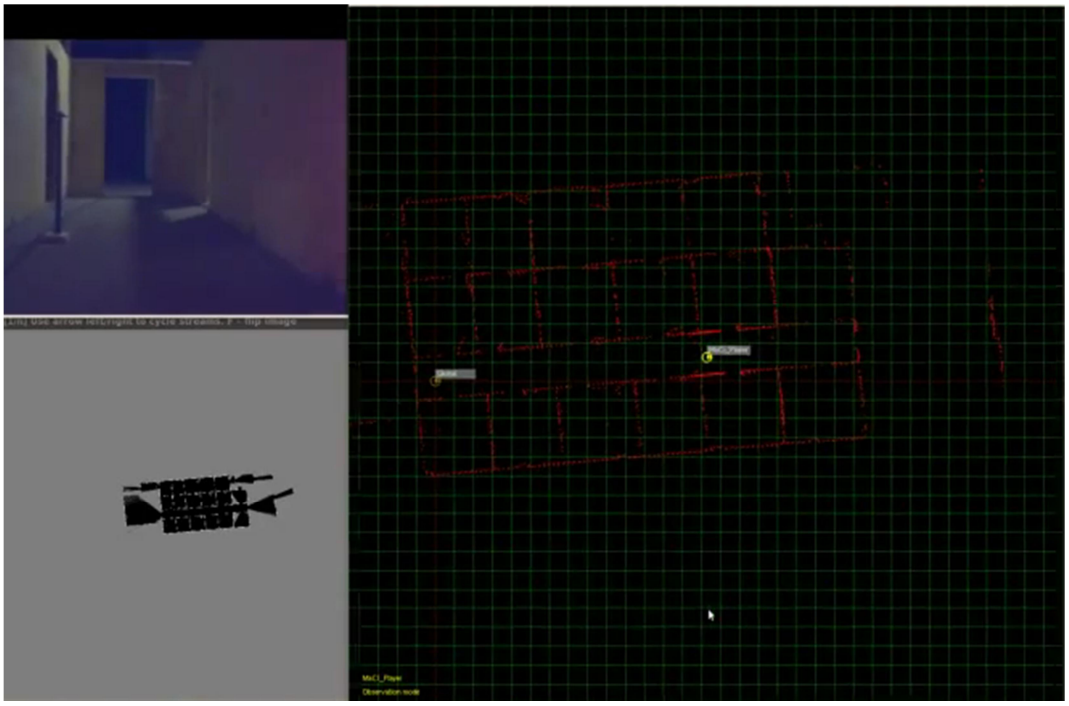

Figure 4.2.2. Teleoperation view for the mobile robot.

As a communication link between the robot and the teleoperation station, two Goodmill w24e routers are used. The Goodmill router is especially designed for critical applications where broadband and reliable connectivity with largest possible coverage is needed. It has different kinds of radio terminals, which can be used depending on the situation, such as 3G HSPA, CDMA450/2000, WiMAX, Wi-Fi, LTE, Flash-OFDM, TETRA (Trans-European Trunked Radio, a radio specifically designed for use by government agencies and emergency services) or satellite. The router monitors continuously all installed WAN radios and switches to another radio if one radio fails or the quality of service is below user determined threshold. In the deployment, two different 3G connections were employed to ensure connection during the operation. In addition, the router supports VPN functionality, which enables secure and seamless connection, independent of the used radio terminal.

The robot uses the GIMnet communication architecture [6, 7], which is a service-based communication middleware for distributed robotic applications. In the application point-of-view, GIMnet provides a virtual private network where all participating nodes may communicate point-to-point using simple name designators for addressing. Using the Goodmill router and the communication architecture, the system provides the possibility to seamlessly control the robot from virtually any remote location. The setup is mostly the same as introduced in [8]. The main difference is the number of the Goodmill's router and the radio terminals used in the router. Another difference is that now the position of the robot as well as the constructed map are also passed to the COP server (see section 4.7) and to the node distribution node (see section 4.3) through ICEStorm as it was chosen as the data management framework of the whole WISM II system [1].

4.3 Deployable Sensor Network

We used the UWASA Node [9] as a sensor platform in our deployable sensor network. We have developed the first version of the node in GENSEN project that was focusing on wireless automation [2]. The modular architecture of the node allows us to easily add several types of industrial sensors depending on our measurement needs. In the case of this project we selected acoustic sensors, cameras and the radio signal itself. Acoustic sensors were used for speaker identification, cameras for visual sensing and radio signal for device free localization (DFL). Acoustic sensing and cameras are explained in 4.3.1 and 4.3.2, DFL in the next subchapter 4.4.

4.3.1 Acoustic Sensing

Wireless sensor nodes can be equipped with small microphones to collect acoustic samples from the building interior. These samples can then be utilized to detect different types of voices and to perform speaker identification. Unlike speech recognition, speaker identification does not identify the content of the spoken message, but it characterizes the speaker. Every speaker has text and language independent unique features in his speech. These features can be characterized by Mel-Cepstral analysis and then used for person identification by matching the features against the ones which are computed from person's voice samples in a database [10].

A speech signal having N samples is collected into vector

$$x = [x(1) \cdots x(N)]. \tag{4.3.1}$$

The high frequencies of the spectrum, which are generally reduced by the speech production process, are enhanced by applying a filter to each element x(i) of x:

$$x_p(i) = x(i) - \alpha x(i-1) \qquad i = 2, \dots, N \tag{4.3.2}$$

In (4.3.2), α is a pre-defined parameter $\alpha \in [0.95; 0.98]$. The signal is then windowed with a Hamming Window of $L_w = t_w f_s$, where t_w is the time length of the window and f_s is the sampling frequency of the signal [10]. The Hamming-windowed speech signal is collected to matrix Y such that each column in Y contains one window of the signal:

$$Y = [y(i,j)] \qquad i = 1, \dots, L_w \qquad j = 1, \dots, N_w \tag{4.3.3}$$

where L_w is the length of the signal window in terms of number of sample points and N_w is the number of sample points in each window. The Discrete Fourier Transform is applied to each column of Y, and the Fourier transformed results are collected to

$$\tilde{F} = [F(y(1)^T) \cdots F(y(N_w)^T)] \tag{4.3.4}$$

where each each column contains N_{bins} elements, where N_{bins} is the number of bins used in the Discrete Fourier Transform. Since the Discrete Fourier Transform provides a symmetric spectrum, only the first half of each Fourier-transformed signal window is considered. Thus, we get a matrix F, which contains only the first N_{bins} / 2 rows. The power spectrum matrix becomes

$$P_w = [|F(i,j)|^2] \qquad i = 1, \dots, \frac{N_{bins}}{2} \qquad j = 1, \dots, N_w. \tag{4.3.5}$$

The frequencies located in the area of human speech are enhanced by multiplying the power spectrum matrix by a filterbank matrix B_f, which is a filterbank of triangular filters, whose central frequencies are located at regular intervals in the so-called mel-scale. The conversion from the mel-scale to the normal frequency scale is done according to

$$f_{Hz} = 700\left(10^{\frac{F_{melscale}}{2595}} - 1\right). \tag{4.3.6}$$

The smoothened power spectrum is transformed into decibels, and the mel-cepstral coefficients are computed by applying a Discrete Cosine Transform to each column vector in P_{dB} such that each element in C_P becomes

$$C_p(k,l) = a(k)\sum_{i=1}^{\frac{N_{bins}}{2}} P_{dB}(i,l)\cos\left(\frac{\pi(2i-1)(k-1)}{N_{bins}}\right), \tag{4.3.7}$$

where $1 \leq k \leq N_{cep}$; $1 \leq l \leq N_w$ and

$$a(k) = \begin{cases} \sqrt{\frac{N_{bins}}{2}} & ,k = 1 \\ \sqrt{\frac{4}{N_{bins}}} & ,2 \leq k \leq N_{cep} \leq \frac{N_{bins}}{2} \end{cases}.$$

The first cepstral coefficient of each window is ignored since it represents only the overall average energy contained by the spectrum. The rest of the mel-cepstral coefficients are centered by subtracting the mean of each signal window from it. Thus, we get the centered mel-cepstral matrix

$$C = \begin{bmatrix} C_p(2,1) - \mu_1 & \cdots & C_p(2,N_w) - \mu N_w \\ \vdots & \ddots & \vdots \\ C_p(N_{cep},1) - \mu_1 & \cdots & C_p(N_{cep},N_w) - \mu N_w \end{bmatrix}. \tag{4.3.8}$$

The lowest and highest order mel-cepstral coefficients are de-emphasized by multiplying each column in C by a smoothening vector M. By doing so, we get a smoothened mel-cepstral matrix $C_s = MC$. A normalized average vector of C_s is then computed such that each value $C_N(i)$ in vector $C_N = [C_N(1)\cdots C_N(N_w)]$ is the average of the respective column in matrix C_s normalized to range [0, 1]. The windowed mel-cepstral vectors corresponding to speech portions of the signal in matrix C_s, are separated from the ones corresponding to silence or background noise by using the overall mean of C_N as a criterion. Thus, a matrix C_{sp} containing only the selected column vectors becomes

$$C_{sp} = [C_s(j)|C_N(j) \geq \mu(C_N)]. \qquad j = 1, \dots, N_w \tag{4.3.9}$$

The final mel-cepstral coefficients C_{cep} are computed by taking the row-vise average of C_{sp}:

$$C_{cep} = \begin{bmatrix} \mu\{C_{sp}(1,1) & \cdots & C_{sp}(1,n)\} \\ \vdots & \ddots & \vdots \\ \mu\{C_{sp}(N_{cep}-1,1) & \cdots & C_{sp}(N_{cep}-1,n)\} \end{bmatrix}, \tag{4.3.10}$$

where n ($n \leq N_w$) is the number of columns selected from C_s to C_{sp}. The information carried by C_{cep} is extended to capture the dynamic properties of the speech by including the temporal first and second order derivatives of the smoothened mel-cepstral matrix C_s:

$$\Delta C_s(i,j) = \frac{\sum_{k=-\emptyset}^{\emptyset} kC_s(i,j+k)}{\sum_{k=-\emptyset}^{\emptyset} k^2}, \quad \Delta\Delta C_s(i,j) = \frac{\sum_{k=-\emptyset}^{\emptyset} k\Delta C_s(i,j+k)}{\sum_{k=-\emptyset}^{\emptyset} k^2}. \tag{4.3.11}$$

The mel-cepstral coefficients ΔC_{cep} and $\Delta\Delta C_{cep}$ are computed from the matrices (4.3.11) by following the same procedure as in the computation of C_{cep}. Finally, the mel-cepstral coefficients and their first- and second order temporal derivatives are collected into the feature vector F_s:

$$F_s = \left[C_{cep}^T \quad \Delta C_{cep}^T \quad \Delta\Delta C_{cep}^T\right]. \tag{4.3.12}$$

The feature vector F_s, which has $3(N_{cep}-1)$ elements, characterizes the speaker. The matching of the unidentified voice sample against the samples already stored in the database is based on the similarity between the feature vector of the unidentified sample and the feature vectors of the samples in the database.

The acoustic samples measured by the sensor nodes are short and the sample rate is low compared to the quality that can be achieved with cabled high-quality microphones. Thus, one of the key research topics is to find out how accurate the speaker identification can be when it is based on the voice samples collected by WSN.

Before WISM II project we made an implementation to Mica Z nodes and tested the speaker identification with them [10, 11]. In that case the acoustic samples were collected by the sensor nodes and then transmitted to PC, where the feature vector was computed. A matching accuracy close to 80% was achieved. However, transmitting the raw acoustic samples over the network took quite a bit of resources, and it is also problematic in security point of view. The UWASA Node we are currently using has enough memory and computation power to run the feature vector computation in the node. If only the feature vector would then be

transmitted over the network, the amount of communication required for the speaker identification would be remarkably less. The information security would also be better, because the feature vector alone does not tell much to the third party that may follow the communication. The original plan was to do the feature vector computation implementation to UWASA Node as a part of WISM II project, but due to lack of time that task was dropped and left to the future research.

4.3.2 Cameras

We made camera implementation to UWASA Node by using CMUcam3, which is one of those open software platforms [12]. It provides basic vision capabilities to small embedded systems in the form of an intelligent sensor. CMUcam3 completes the low cost hardware platform by providing a flexible and easy to use open source development environment which makes it a good candidate to work with. Additionally, it is based on LPC2106 microcontroller which belongs to the same family with LPC2378, which is used in the UWASA Node.

CMUcam3 basically consists of two different boards connected to each other with standard 32 pin 0.1 inch headers: the camera board and the main board. The processor, power connections and the FIFO chip of the CMUcam3 are located on the main board while the camera board only consists of a vision sensor and a header connected to sensors pins [13]. The hardware architecture of CMUcam3 is presented in Figure 4.3.1.

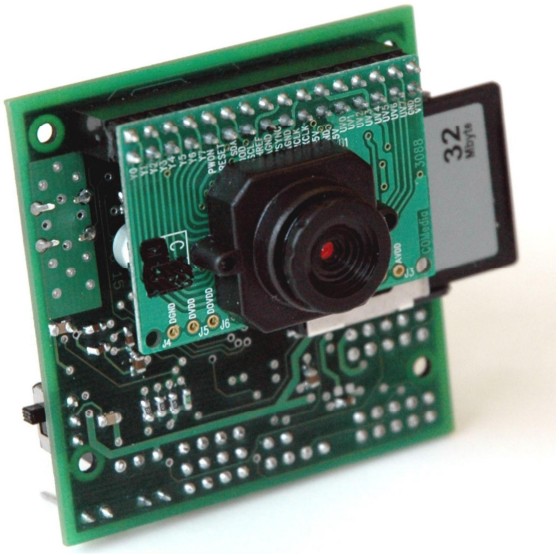

Figure 4.3.1. CMUCam3 with camera board in the front [13].

In this design, only the camera board of the CMUcam3 is used as vision sensor. This architecture aims to enable easy replacement of the vision sensor depending on the application requirements. Since the behavior of this slave module reflects all of the hardware related features of CMUcam3, it may also be possible to substitute the camera board with another one having different specifications.

The camera board of CMUcam3 is a portable PCB circuit that integrates some passive components, OV6620 vision sensor, and a header. Header represents some of the vision sensor pins to external devices. The vision sensor OV6620 is able to output images at a maximum resolution of 352 x 288 pixels up to 60 fps. It can be configured via SCCB interface to output in 8 bit or 16 bit, RGB or YCbCr colour modes. The maximum power consumption of the camera is 80 mW and it operates at 5 V DC. In UWASA Node implementation, a DC to DC conversion from 3.3 V to 5 V is necessary [12].

4.3.3 Sensor Node Deployment Device

A node deployment device was designed and implemented to the mobile robot to enable it carry and deploy static sensor nodes. The circuit board of the node deployment device consists of an ATMEL ATmega16 microcontroller, a MAX232 chip and of a voltage regulator. The Atmega16 microcontroller has four Pulse Width Modulation (PWM) channels that are used to control the four servo motors. To enable the communication between the embedded PC of the mobile robot and the ATmega16 microcontroller, a MAX232 is needed in order to convert the RS232 signal to an UART signal and vice versa. A voltage regulator is needed in case the input voltage exceeds 5V.

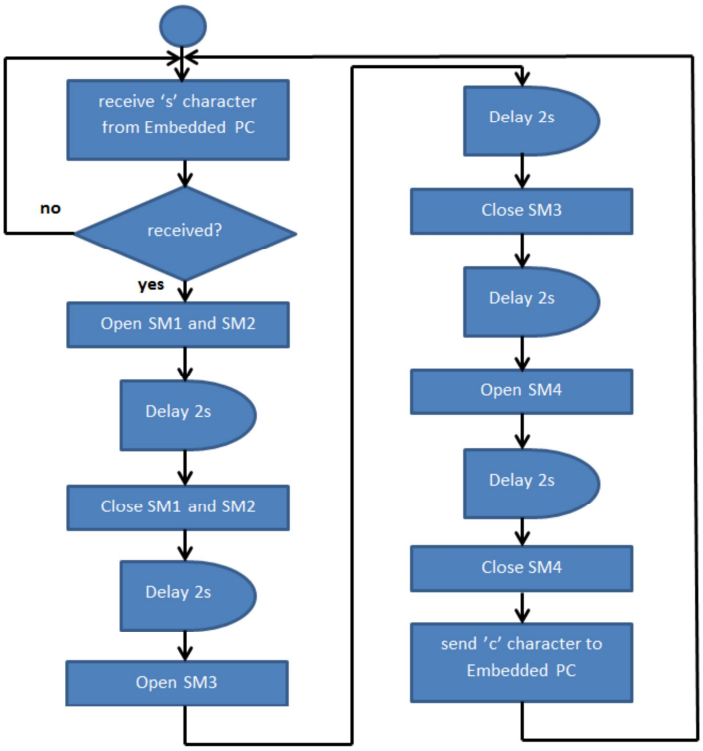

Figure 4.3.2. Flowchart of the node deployment device.

The software of the node distribution device is implemented according to Figure 4.3.2. First the program waits until it receives a start command from the Embedded PC. If a start command is received then the servo motors (SM1 and SM2) at the bottom of the device will open so that the wireless node drops down to the ground. After a certain delay time the servo motors (SM1 and SM2) will close. Then the servo motor (SM3) above servo motor (SM1) will open. After a certain delay time it will close and the other servo motor (SM4) above servo motor (SM2) will do the same procedure. Finally a complete command is sent to the embedded PC.

4.4 Device Free Localization

Wireless sensor networks (WSNs) are finding their way into a new type of sensing where the wireless medium itself is probed using the communications of a dense network deployment. Such networks are referred to as RF sensor networks [14] since the radio of the low-cost transceivers is used as the sensor. RF sensor networks do not require people to co-operate with the system, allowing one to gain situational awareness of the environment non-invasively. Consequently, RF

sensor networks are rendering new sensing possibilities such as device-free localization (DFL) [15].

Wireless networks are ubiquitous nowadays and wherever we are, we are interacting with radio signals by shadowing, reflecting, diffracting and scattering multipath components as they propagate from the transmitter to receiver [16]. As a consequence, the channel properties change due to temporal fading [17], providing information about location of the interacting objects and about the rate at which the wireless channel is altered. To quantify these changes in the propagation medium, one could for example measure the channel impulse response (CIR) [14].

The CIR allows one to measure the amplitude, time delay, and phase of the individual multipath components, but requires the use of sophisticated devices. In the context of situational awareness and locating non-cooperative objects, the time delay is the most informative. For example, in the simplest scenario when there exists' one multipath component in addition to the line-of-sight (LoS) path, the excess delay of the reflected component specifies that an object is located on an ellipse with the TX and RX located at the foci [18]. Furthermore, the difference between the excess delays of consecutive receptions determines the rate at which the wireless channel is changing.

Devices capable of measuring the CIR can be prohibitively expensive, especially when compared to low-cost narrowband transceivers. As a drawback, these low-complexity narrowband devices are only capable of measuring the received signal strength (RSS) which is a magnitude-only measurement. Nevertheless, also the RSS provides information about the surrounding environment. First, when a dominating LoS component is blocked, RSS tends to decrease, indicating that a person is located in between the TX-RX pair [15]. Second, variance of the RSS indicates changes in multipath fading [19] and therefore, about the location of people and the rate at which they are interacting with the propagation medium.

Despite the fact that narrowband transceivers are not as informative as devices capable of measuring the CIR, one can leverage low-cost of the devices and deploy them in numbers to gain situational awareness. For example, temporal fading information from a dense RF sensor network can be exploited to perform DFL [15, 20], a research topic addressed in the context of WISMII project. In the following, we describe the development efforts conducted during the project.

4.4.1 Requirements of Device Free Localization

Thus far, in the context of RSS-based DFL, the research has mainly focused on developing models and algorithms to be used for extracting location information from the RSS measurements of the many static links of the wireless network. These systems are typically deployed for a short time period [15, 19, 20]. However, requirements of real-world deployments are often neglected such as: varying communication conditions [21], fault management [22] and energy efficiency [23]. In the future, when DFL systems are integrated as part of larger systems to provide position based content, the importance of these requirements increases and in such deployments, network management must be addressed.

The operation principle of the DFL system is based on the assumption that the RSS of each node in the network are affected by a person who remains in the same location. This assumption of the DFL algorithms put stringent optimization constraints on the network development due to physical properties of the wireless channel. However, the rich literature on network management for constraint devices [24, 25, 26] rely on network and transport layer specification so that the management functionality is considered in the application layer, which has considerable processing overhead. Thus, the proposed network management solutions cannot be utilized in DFL systems without sacrificing the performance.

Network management serves three purposes in DFL: first, the network can be configured easily reducing deployment time; second, adapting to the changing communication conditions, i.e., the network can change the frequency channel of operation if needed; third, it enables energy efficient networking, i.e. the system can go to sleep while the area is not occupied or changes of interest are not encountered. In real-world DFL deployments network management is mandatory. A management framework based on the unique and stringent constraints of DFL networks, which leverages the DFL performance while providing network management functionality is presented in [27]. In the following, we highlight the main requirements of the proposed management framework and present the solution.

System Overview

It is well known that propagating radio waves are altered by the medium, which is observed through the amount of experienced losses. Despite the fact that there are many sources of propagation losses, link shadowing is of particular interest since the human presence in the medium cause’s additional attenuation in the signal. Further, nodes in close proximity of one another experience correlated shadowing, which depends on the position and geometry of the shadow [28]. As in computerized tomographic imaging [29], the distribution of shadowing losses in an

area of interest can be determined using the signal strength measurements of a dense wireless network [15]. Therefore, DFL is frequently referred to as RF tomography [30, 31] or radio tomographic imaging (RTI) [15, 32].

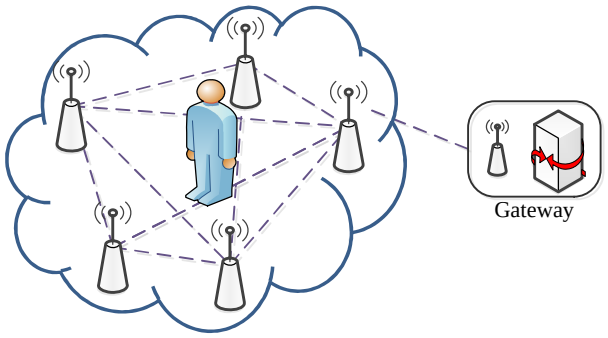

Figure 4.4.1. DFL system overview.

In general, a DFL system is composed of a dense wireless network and a gateway as shown in Figure 4.4.1. The network is formed by nodes which are placed in predefined positions and allowed to communicate with each other in a prescribed manner. The gateway is simply a computer attached to the sink node, which is capable of sniffing the ongoing communication in the network. The aim of the system is to determine the location of the person in Figure 1 using the RSS measurements of the nodes. For this purpose, the network typically follows a simple transmission schedule such that at a given time instant only one of the nodes is transmitting while the others are listening. Although measuring the RSS does not require transmitting any specific type of packets, the scheduled node typically broadcasts the most recently acquired measurements so that the sink node receives and relays these measurements to the computer. The computer stores the data for later use and/or constructs the images of the shadowing field and/or estimates the locations of people online.

Physical Constraints of DFL

A propagating radio wave is altered by reflection, diffraction, scattering and waveguiding in addition to free space propagation [33, Chapter 4]. In general, stochastic models are utilized to represent all of these mechanisms and a distinction is drawn between the losses due to small scale and large scale effects. The large scale losses are widely represented by a power law, which can be extended to cover the shadowing losses of a link by modeling this as a weighted line integral of a loss-field [28]. In this model, each point on the line joining the transmitter and receiver (link line) has a weighted contribution on the shadowing losses. Thus, the model explicitly explains the correlation among two links with an im-

plicit dependence on the position and geometry of the shadow. The correlation among different links allows estimating the loss field using a finite amount of RSS measurements. As the number of correlated measurements modulated by the same shadowing source increases, the distribution of the loss-field in the traversed area can be estimated. For example, the RSS measurements of a dense wireless network are affected by the same loss-field, which render a convenient measurement system enabling the localization of the shadowing source.

The acquired RSS measurements are not only effected by shadowing. On the contrary, they reflect the overall effect of small scale, large scale and shadowing losses. Thus, the accuracy of shadowing loss-field estimation depends on the level of shadowing loss information that can be extracted from the measurements. The effect of other losses can be averaged out by increasing the number of measurements affected by the same shadowing loss field. For example, a significant improvement in accuracy is achieved by collecting measurements on multiple frequency channels [20]. However, the loss field varies both in time and frequency in accordance with the physical characteristics of the wireless channel. More specifically, the coherence bandwidth and coherence time of the channel define the limits of the maximum frequency separation among the channels, and the maximum time delay between samples [34]. Within these limits, the wireless channel can be considered constant and the loss-field can be estimated accurately. As a drawback, the intrinsic broadcast nature of the wireless communication does not allow simultaneous transmissions on the same frequency channel, which dictates a schedule for the network depending on the coherence bandwidth and coherence time of the channel. Therefore, the accuracy of DFL has a strong dependence on unknown properties of the wireless channel and on the transmission schedule of the network.

Ideally, the location of the people can be determined in arbitrarily high resolution by increasing the density of the network either by decreasing the distance between the nodes (decreasing the area of interest) or by increasing the number of nodes. However, the distance between receivers also affects the correlation among the small scale fading components that neighboring nodes encounter. Hence, the positions of the nodes in the network cannot be selected considering only the resolution concerns, but also the physical limitations imposed by other loss sources.

In summary, the shadowing-loss field can be estimated by signal strength measurements of a dense wireless network. However, the performance depends strongly on physical placement of the nodes and the properties of the wireless channel, which is not known prior to deployment. The accuracy of DFL can be improved by increasing the number of measurements acquired for the same shadowing

field, either by increasing the number of nodes or the frequency channels used for communication. However, in either case, latency of successive measurements increases making it harder to satisfy the requirements dictated by the coherence bandwidth and coherence time. Therefore, a highly accurate DFL system can only be achieved by using the signal strength measurements of a tightly managed wireless network, which provides moderate level of configurable features in order to adapt the measurement system to the varying channel conditions.

Networking Requirements

The wireless network of a DFL system has a mesh topology, where the system monitors an area within the transmission range of the nodes. In general, a DFL network follows a transmission schedule and does not require a sophisticated networking paradigm. The physical (PHY) layer specification handles most of the communication problems arising from the mobility in the medium, such as carrier and symbol synchronization [35]. The coverage and connectivity problems of such a network are addressed by the mechanisms of the medium access control (MAC) specification. Moreover, the underlying communication does not need to follow sophisticated network layer rules for routing and convenient data exchange mechanisms because of the topology. However, a DFL system needs to provide mechanisms to acquire as many measurements as possible modulated by the same loss-field.

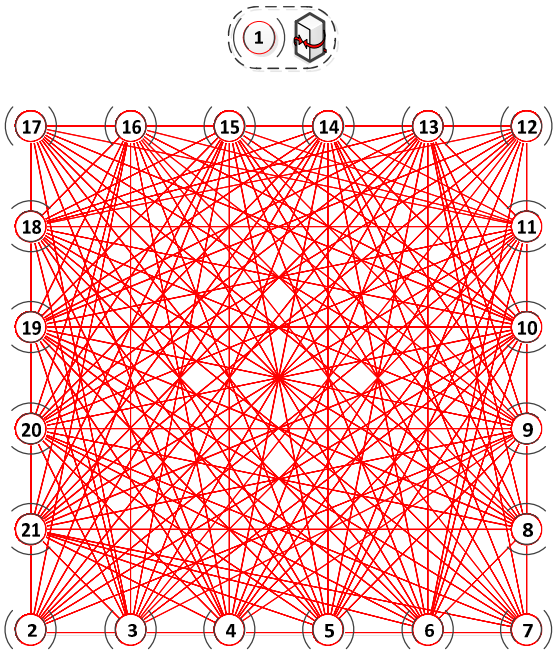

Figure 4.4.2. DFL network topology.

The connectivity graph of a DFL network is shown in Figure 4.4.2. Since each broadcast must be received by all the neighbors, the transmissions must obey the time division multiple access (TDMA) rules and/or must follow round-robin (R-R) like transmissions. In either case, the transmission turn is assigned based on the unique node ID as shown in Figure 4.4.2. The sink node (ID 1) is the first in schedule and it begins every round of communication. In TDMA implementations, each node in the network transmits at its own time slot. In a pure R-R schedule there is no strict time slot for transmissions, but they are triggered by a reception from the previous node in schedule. Furthermore, since in most of the considered deployment scenarios the wireless channel tend to have a wide coherence bandwidth, the network can communicate in different frequency channels to alleviate the accuracy of the system. Therefore, a typical DFL network requires a schedule, which determines the participating nodes, the order of the medium access, and the frequency channel(s) of transmissions, while keeping the delay between transmissions minimal.

The DFL imaging algorithms are typically executed after all the nodes in a schedule broadcast their measurements, which corresponds to a complete set of measurements or a round of measurements. As the imaging algorithms require minimal time delay between successive transmissions in a round, either the TDMA MAC must have very narrow time slots and/or the transmissions must be scheduled in R-R fashion. In case static schedules are used, completion of a round triggers the next round of communication. Therefore, the energy constraints are neglected since the nodes are not allowed to change their power mode. Furthermore, since a DFL network relying on a static schedule cannot counteract to variations in the channel, the system is at most best-effort. In such a system, all the nodes must participate to every communication event, which increases the durations of the measurement round but also the energy requirements linearly with respect to the number of nodes and frequency channels. In contrast, a DFL system allowing dynamic scheduling can adaptively alter the number of frequency channels and the nodes participating in a round of communication by keeping track of the state of the system using the output of the imaging algorithms. In summary, an energy efficient DFL system suitable for long-term deployments requires dynamic scheduling which takes into account the state of the imaging subsystem as well as the energy constraints of the nodes.

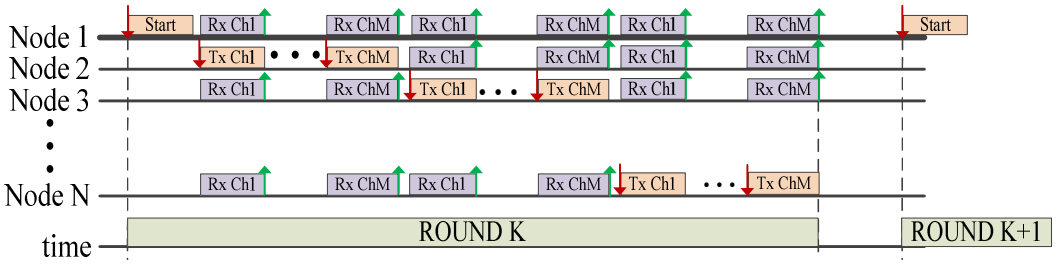

Figure 4.4.3. Measurement coordination in a DFL network.

A measurement round fulfilling the requirements listed above is shown in Figure 4.4.3, where the receptions and transmissions are represented by up and down arrows, in respective order. For each round, the start is marked by the sink node, and each node follows the transmission schedule. The coordination commands must be distributed to the nodes at beginning of each round along with start command transmission. The nodes must be able to keep track the state of the round, and perform specific actions according to the state such as reconfiguring the operation mode, switching the frequency channel, enabling receivers or transmitters, generating measurement packages, and transmitting a suitable packet. In this approach, a round data is composed of measurements from different frequency channels in order to minimize the time delay between measurements. Furthermore, the configuration distribution is aligned with the start of the round so that the measurement coherency is maintained, while the nodes that are not taking part in a round can change their power mode. Consequently, a medium access scenario depicted in Figure 4.4.3 is a candidate implementation for DFL network supporting dynamic scheduling.

DFL as a Subsystem

The DFL system can act as a part of a larger system, for example, as a passive localization subsystem of a home automation system, or ambient assisted living system. Furthermore, since the information shared in the network is not restricted, the DFL network can be utilized to collect pervasive data or to distribute some specific action commands. On the other hand, the network monitoring feature of the gateway may generate alerts to the global system operator to alleviate quality of service. Thus, the gateway must be able to share the information between different subsystems, and perform specific actions according to state of or commands from the global system.

4.4.2 Network Coordination and Management

For short-term deployments, the networking requirements listed in the preceding subsection and the need for network configuration and management are irrelevant. However, for long-term deployments the wireless network requirements identified in the preceding subsection imply a tightly coordinated network. In addition to the coordination needs for the medium access, the energy concerns render centralized management requirements. For a DFL network, with topology shown in Figure 4.4.2, the gateway is the only one to fulfill these coordination and management requirements since the complete measurement data is not available to other entities of the network. Therefore, the gateway does not only act as an infinite memory attached to the sink node, which listens to the ongoing communications but also as a network coordinator and manager.

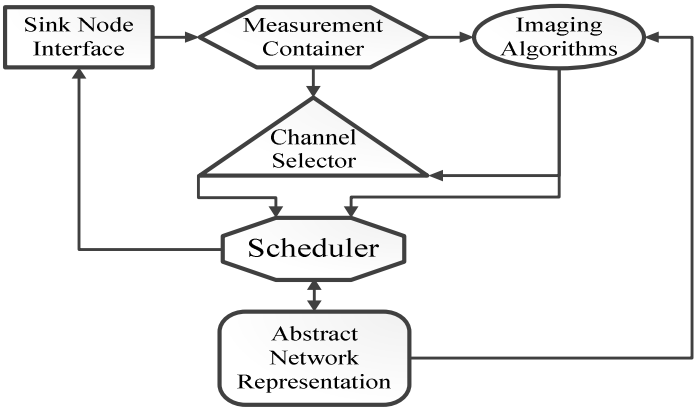

Figure 4.4.4. Coordination components of the gateway.

The coordination tasks of the gateway are tightly coupled with cooperation among different system components to allow online DFL imaging and energy efficient operation as shown in Figure 4.4.4. The network coordination task is performed by an adaptive scheduler, which requires an input from the imaging subsystem, and the frequency channel ranking (channel selector) subsystem. Thus, the acquired RSS measurements are used for both imaging and networking purposes. As the generated schedule must be known also by the imaging algorithm for proper shadowing loss-field estimation, the generated schedules are shared through the component storing the abstract representation of the network. The generated schedule is broadcasted to the network through the sink node.

The utilization of battery-powered, low-energy and low-cost wireless networks brings forth reliability concerns, as the long-term operation of these systems depends upon multitudes of low-cost subsystems. As argued by Tolle and Culler

[36], long-term deployments require tight monitoring and expert-system like alerting functionality implemented as an integral component of the gateway. The number of links in a DFL network is quadratic with number of nodes, which also increases linearly with the number of channels used for communication making it impossible for an operator to track the status of the network without monitoring aids. On the other hand, these networks must also provide hard configuration modification options to allow the operator to interfere with the system if necessary. The monitoring and configuration options of the gateway constitute the network management components, whose interrelations are depicted in Figure 4.4.5.

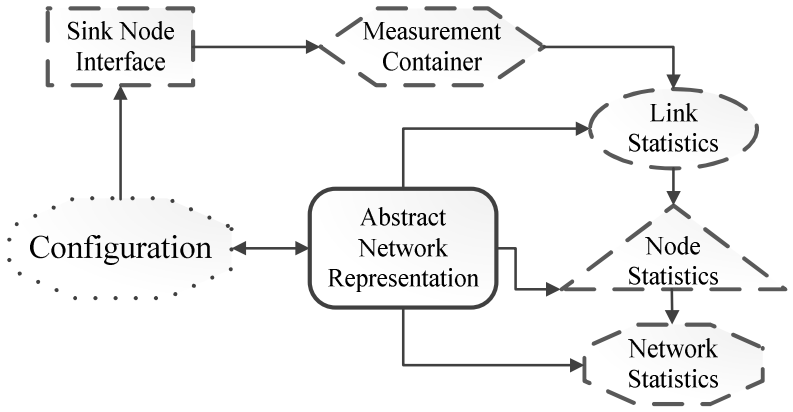

Figure 4.4.5. Management components of the gateway.

DFL and Network Management Gateway

The gateway has four main functions as network coordinator, network manager, global system client, and DFL imaging subsystem. In addition to these functional components, the implemented gateway software has rich set of user interface and data logging features, as depicted in Figure 4.4.6. The acquired network data is shared with the data logger and with the abstract node, which relays the measurement to the measurement container of its links while logging the node specific data. After completing a round of measurements, the user interfaces are refreshed with the new status, and the imaging block is activated to update the estimates using the new measurements. The output of the imaging subsystem is redirected to the global system and to the image display. The configuration is checked and/or updated by the scheduler before starting a new round.

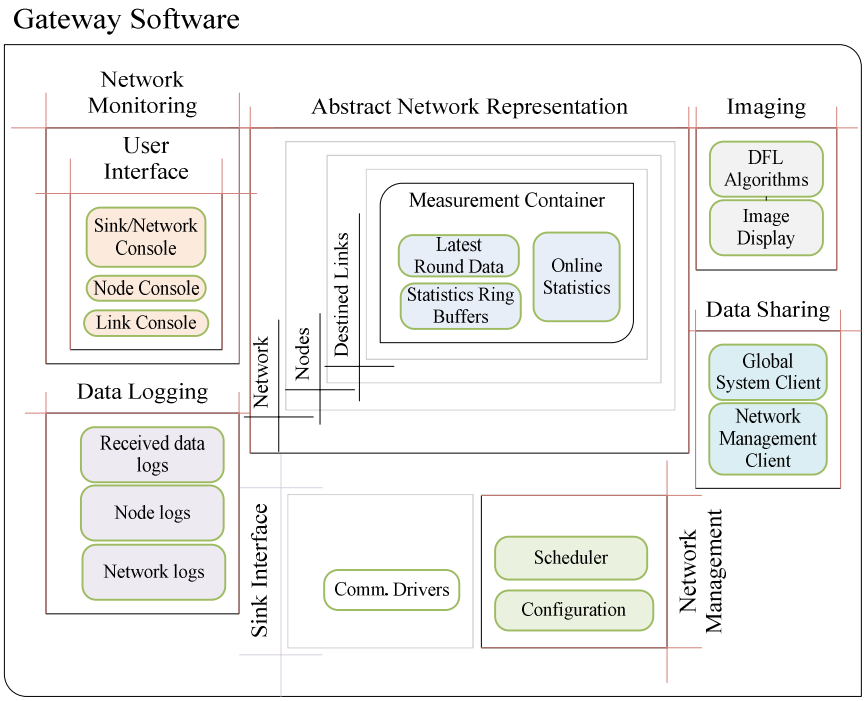

Figure 4.4.6. Gateway software components.

4.4.3 Radio Tomographic Imaging

In the following, we describe radio tomographic imaging (RTI), a technology that enables DFL. As stated before, changes in the propagation characteristics of the monitored area alter the RSS measurements. This change can be induced e.g. by moving people, opening and closing of doors/windows, furniture replacement, etc. Generally, variations in RSS are the largest when changes occur in between or in the close proximity of the transmitter and receiver. We measure the RSS change of link l at time k as

$$y_l(k) = \bar{r}_l - r_l(k), \tag{4.4.1}$$

where $\bar{r}_l$ is the reference RSS measured when the link is not obstructed and $r_l(k)$ is the current measurement. The measurement vector of the L wireless links is $\boldsymbol{y} = [y_1, \cdots, y_L]^T$

The objective of RTI is to estimate a discretized image $\boldsymbol{x}$ of size $N \times 1$ describing the changes in the propagation field, from the measurement vector $\boldsymbol{y}$. Pixel of the discretized image, denoted by x_n, represents the amount of RSS change occurring inside pixel n. As in [15, 30], we assume that $\boldsymbol{y}$ is a linear function of $\boldsymbol{x}$

$$\boldsymbol{y} = \boldsymbol{W}\boldsymbol{x} + \boldsymbol{b}, \tag{4.4.2}$$

where $\boldsymbol{b}$ is the measurement noise vector of size $L \times 1$ and $\boldsymbol{W}$ is the weighting matrix of size $L \times N$ with elements

$$W_{l,n} = \begin{cases} \frac{1}{\sqrt{d_l}} & \text{if } d_{l,n}^{TX} + d_{l,n}^{RX} < d_l + \lambda \\ 0 & otherwise \end{cases} \tag{4.4.3}$$

In Eq. (4.4.3), d_l is the distance between the transmitter and receiver, $d_{l,m}^{TX}$ and $d_{l,m}^{RX}$ are the distances from the center of pixel n to the transmitter and receiver of link l respectively, and λ is the excess path length of the weighting ellipse. In Figure 4.4.7, weighting ellipses with different λ values are shown.

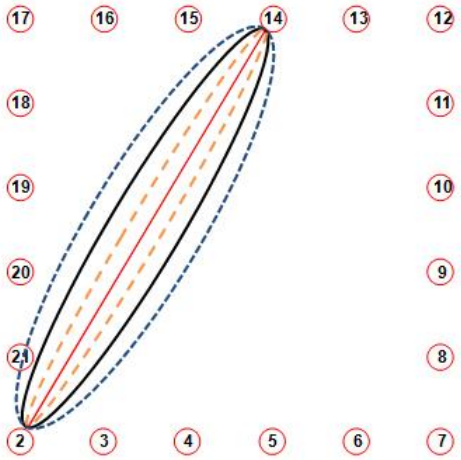

Figure 4.4.7. Weighting ellipses with different λ values.

Estimating the image vector $\boldsymbol{x}$ from the measurements $\boldsymbol{y}$ is an ill-posed inverse problem, thus regularization is required. We assume that the image vector has covariance matrix $\boldsymbol{C}$ for which element i, j is given by

$$C_{i,j} = \sigma_x^2 e^{d_{i,j}/\delta}, \tag{4.4.4}$$

where σ_x^2 is variance of the pixel, $d_{i,j}$ is the distance between pixels i and j, and δ is the pixel correlation distance. To form the image, a regularized least squares approach is used [20, 30, 32]

$$\hat{\boldsymbol{x}} = \boldsymbol{\Pi}\boldsymbol{y}, \quad \boldsymbol{\Pi} = (\boldsymbol{W}^T\boldsymbol{W} + \boldsymbol{C}^{-1})^{-1}\boldsymbol{W}^T. \tag{4.4.5}$$

The linear transformation $\mathbf{\Pi}$ must be only computed once and it enables real-time image reconstruction via Eq. (4.4.5). The linear model for shadowing loss is based on the correlated shadowing models in [28, 30], and on the work presented in [15].

4.4.4 Enhancing the Accuracy of RTI

RTI, as it was introduced in the preceding section, assumes that the movement of a person affects the RSS measurements only when the person is very near the line connecting two communicating transceivers [15, 19]. In addition, it is presumed that when a person's presence is exactly on this line between transceivers, which we call the link line, the sensors will strictly observe attenuation [15, 31, 37]. In open environments where LoS communication among the nodes is dominant and in networks where the distance between the nodes is small, both assumptions are valid. However, for cluttered environments and longer sensor distances, the two assumptions do not apply. In obstructed environments, the RSS of a link can both increase or remain unchanged as the link line is obstructed [19, 38]. In addition, as the signals propagate via multiple paths from the transmitter to the receiver, it is plausible that a person located far away from the link line affects a subset of multipath components by reflection [39] or scattering [40], inevitably causing a change in RSS. For these reasons, channel diversity [20] and more accurate models to characterize the spatial impact area in which a person's presence affects the RSS [41] have been studied.

Channel Diversity

The relation between steady-state, narrow-band fading and the temporal fading statistics of the RSS due to human movement is described in [38]. The authors define fade level, a continuum between two extremes, namely a *deep fade* and an *anti-fade*, for the fading observed on a wireless link. A link in a deep fade is affected by destructive multipath interference and will most probably experience high variance as the person moves in a wide area near the transmitter and receiver and the line in between them. In addition, a deep fade link's RSS on average increases when the LoS is obstructed. On the contrary, a link in an anti-fade is affected by constructive multipath interference. The RSS of these links varies significantly less due to movement in the area. As their LoS is obstructed, anti-fade links' RSS tends to decrease. Anti-fade links are the most informative for DFL because the area in which a person changes the RSS is small and predictable, largely limited to the straight line between the transmitter and receiver. We use $\bar{r}_{l,c}$ as a measure of the fade level – if $\bar{r}_{l,c1} < \bar{r}_{l,c2}$, the link is said to be in a deeper fade in channel $c1$ than in $c2$.

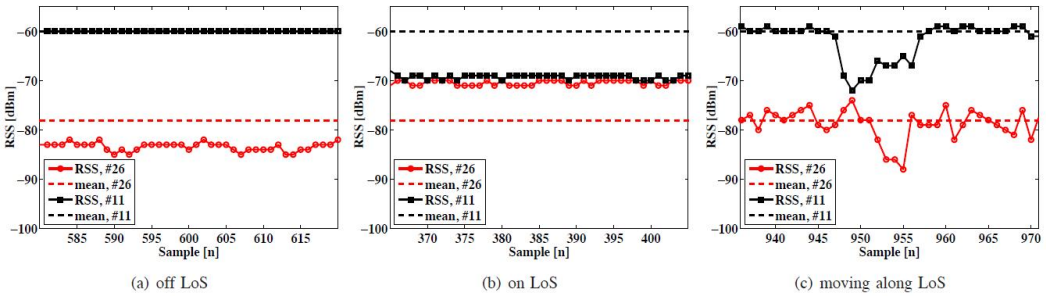

Figure 4.4.8. Temporal fading of the RSS on two different channels due to human movement, when the line between the TX and RX is not obstructed (a), and is obstructed (b). In (c), the person moves in between the nodes, walks along the link line, and then moves away from the nodes.

To illustrate the effect of fade level, Figure 4.4.8 plots the RSS measurements on two different channels of a single link. The dashed lines in Figure 4.4.8 (a)-(c) show the mean RSS during the calibration period. It can be observed that the fade level difference between the two channels is almost 20 dBm. The link can be considered to be in anti-fade on channel 11 and in deep fade on channel 26.

The solid lines graphed in Figure 4.4.8 (a) show the RSS when the person is standing 4.5 meters away from the LoS. On channel 11, the RSS is the same as the one measured during calibration. In contrast, the deep fade channel measures attenuation even though the LoS is not obstructed. In Figure 4.4.8 (b), the solid lines show the RSS when the person is standing on the LoS. It can be observed that the anti-fade channel experiences attenuation, whereas the deep fade channel experiences an increase in signal strength. In Figure 4.4.8 (c), the person is walking towards the link line reaching the LoS of the link at sample 948, walks along the LoS and finally moves off the LoS at sample 958 and then walks away from the link line. In this case, the anti-fade channel measures a small RSS variation until the LoS is obstructed and a constant attenuation while the person is moving along the LoS. Once the person leaves the LoS, the RSS goes back to the mean value. On the contrary, the deep fade channel starts varying already before the LoS is obstructed, and measures RSS values both higher and lower than the mean while the person is moving along the LoS. Once the person moves away from the LoS, the deep fade channel's RSS continues to vary.

From this example and evidence from the literature [19, 38], we see that links in a deep fade are not reliable indicators of the presence of a person on the line between the transmitter and receiver. In addition, in obstructed indoor environments, multipath fading is severe and anti-fade links are few. An RTI system that relies on any one channel will have few links accurately measuring person loca-

tion. On the other hand, when channel diversity is used as proposed in [20], the number of anti-fade links can be considerably increased, consequently improving RTI's localization accuracy.

Fade Level -based Spatial and Measurement Models

As shown in Figure 4.4.8, the linear model for shadowing loss is inaccurate for channel 26 and therefore, more accurate spatial and measurement models to enhance the performance of RTI have been proposed [41]. In the work, the spatial impact area where human-induced RSS changes are measured is identified to vary considerably for each link of the RF sensor network. Moreover, the spatial impact area is also identified to depend on the sign of RSS change, i.e., even for the same link and channel, increases and decreases of the RSS are observed over different spatial areas. As a result, based on extensive experiments, a measurement model is proposed which captures the human-induced RSS changes more precisely. In addition, a spatial weight model is introduced which more accurately relates the measurements to the true location of the person. The models are built upon the concept of fade level and in the paper, it is demonstrated that the more challenging the environment is for localization, the greater the enhancement in accuracy is. In the following, we present the derived models.

The image reconstruction procedure for RTI can be used as a theoretical framework for estimating the changes in the RF propagation field with the fade level-based spatial weight and measurement models [41]. However, minor adjustments need to be made to RTI as it was introduced in Section 4.4.3. First, instead of applying the changes in RSS as given in Eq. (4.4.1), we apply the probability of the person being located inside the modeled ellipse

$$p_{l,c}^{\Delta}(k) = 1 - e^{-\beta_{l,c}^{\Delta}|\bar{r}_{l,c} - r_{l,c}(k)|}. \tag{4.4.6}$$

Table 4.4.1. Parameters of the fade level-based spatial weight and measurement models.

Parameter	$\Delta\ is -$	$\Delta\ is +$
k_{λ}^{Δ}	-5.79	102.73
b_{λ}^{Δ}	0.21	0.50
k_{β}^{Δ}	Inf	13.00
b_{β}^{Δ}	0.12	0.18

For RSS change direction Δ, $\beta_{l,c}^{\Delta}$ in Eq. (4.4.6) is given by

$$\beta_{l,c}^{\Delta} = b_{\beta}^{\Delta} \cdot e^{F_{l,c}/k_{\beta}^{\Delta}}, \tag{4.4.7}$$

where $F_{l,c}$ is the fade level, and b_{β}^{Δ} and k_{β}^{Δ} are given in Table 1. The difference between a radio propagation model and the mean RSS of link l and channel c, is what we call fade level

$$F_{l,c} = \bar{r}_{l,c} - P(d), \tag{4.4.8}$$

where $P(d)$ is a model for the RSS vs. distance. In a wireless network, the RSS can be modeled e.g. using the log-distance path loss model [34]

$$P(d) = P_0 - 10\eta \log_{10} \frac{d}{d_0}, \tag{4.4.9}$$

where P_0 is the reference loss at a short reference distance d_0, η the path loss exponent, and d the distance between the transceivers. Now, based on the measured sign of RSS change and fade level of the link, the new measurement vector on frequency channel c when attenuation is measured is $\boldsymbol{y}_c^- = [p_{1,c}^- \ , \cdots , \ p_{L,c}^-]$. Correspondingly, for measured increases $\boldsymbol{y}_c^+ = [p_{1,c}^+ \ , \cdots , \ p_{L,c}^+]$, thus, the complete measurement vector on frequency channel c becomes $\boldsymbol{y}_c = [\boldsymbol{y}_c^- | \boldsymbol{y}_c^+]$. When considering all the channels, the complete measurement vector is $\boldsymbol{y} = [\boldsymbol{y}_1 | \ \cdots \ | \boldsymbol{y}_C]^T$, where C is the number of frequency channels used for communication.

The excess path length λ of the weighting ellipse is also a function of fade level and sign of RSS change. In [41], the following relationship was derived

$$\lambda_{l,c}^{\Delta} = b_{\lambda}^{\Delta} \cdot e^{F_{l,c}/k_{\lambda}^{\Delta}}, \tag{4.4.10}$$

where b_{λ}^{Δ} and k_{λ}^{Δ} are given in Table 1. Now, the spatial weighting model in Eq. (4.4.3) has to be reformulated since λ is unique for each link and channel. The new weight model can be mathematically expressed as

$$W_{l,c,n}^{\Delta} = \begin{cases} \dfrac{1}{A_{l,c}} & \text{if } \ d_{l,n}^{TX} + d_{l,n}^{RX} < d_l + \lambda_{l,c}^{\Delta} \\ 0 & otherwise \end{cases} \tag{4.4.11}$$

where $W_{l,c,n}^{\Delta}$ is the weight of voxel n for link l on channel c for RSS change direction Δ. Because the area covered by the ellipses varies, we weight less the links that cover a larger area by setting the weight to be inversely proportional to the

area of the ellipse, i.e., $A_{l,c}$. The regularized least-squares approach in (4.4.5) can be used with the new models for image reconstruction.

4.4.5 Online RSS Calibration

The different methods used in RSS-based DFL, e.g. [15, 20, 31, 37], must learn the reference characteristics of the RSS on each link while a person is not nearby to be able to quantify the change when a person is located near the link. However, the baseline characteristics of RSS change over time as the surrounding environment is altered [42]. For this reason, a DFL system has to adapt to the changes in the monitored area and recalibrate online the reference RSS of the links in order to guarantee a high localization accuracy over an extended period of time. Besides the traditional challenges associated with enabling reliable communication in long-term wireless network deployments, the DFL system must be able to accurately measure changes in the radio environment without requiring any manual recalibration, reconfiguration, or restarting, even if any particular node fails. For this reason, online algorithms have been investigated to adapt to the changes in the environment [32, 42].

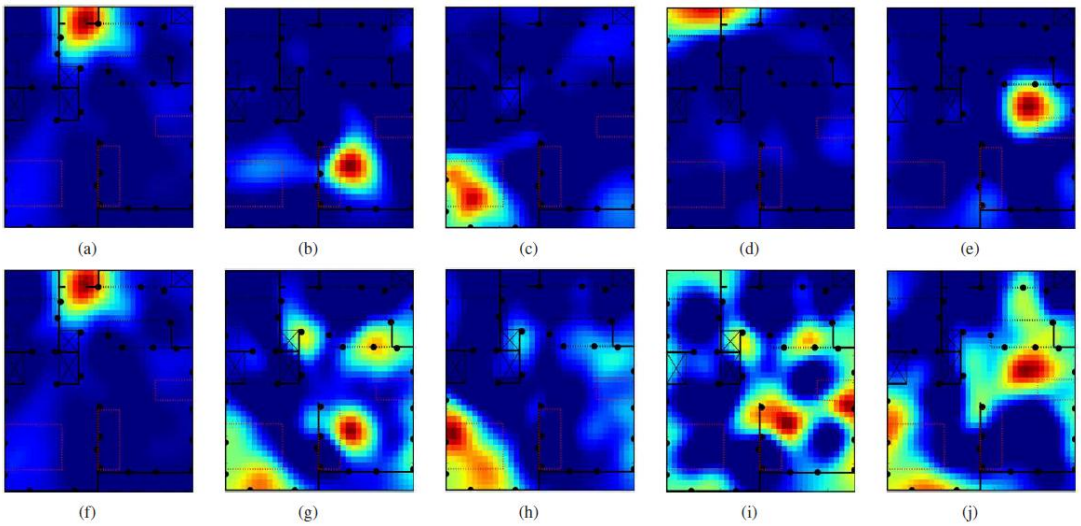

Figure 4.4.9. Attenuation images obtained when the reference RSS is updated online (a)-(e) and when it is not updated after an initial calibration (f)-(j). Starting from the left, the images are plotted over one day in 6 hours intervals: in (a) and (f), the person is located at the entrance, in (b) and (g) on the sofa, in (c) and (h) in bed, in (d) and (i) in the bathroom and in (e) and (j) by the table of the apartment. When the reference RSS is not up dated, the images become noisy over time due to changes in the radio signal propagation patterns, eventually providing wrong position estimates, as in (i).

In [32], the reference RSS $\bar{r}_{l,c}(k)$ is calibrated online using a moving average

$$\bar{r}_{l,c}(k) = (1-\alpha)\cdot \bar{r}_{l,c}(k-1) + \alpha \cdot r_l(k), \tag{4.4.12}$$

where $\alpha \in [0,1]$ is a parameter defining the rate of adaptation of the reference RSS. In Figure 4.4.9, the effect of online calibration is shown in an apartment deployment. In Figures 4.4.9 (a)-(e), attenuation images obtained by applying the moving average and RTI, as explained in Section 4.4.3, are shown. With this method, the system is capable of adapting to the varying environment. When the radio signal propagation patterns change, due to e.g. opening and closing of windows or movements of objects, the system dynamically adjusts the reference RSS of the lines traveling across the monitored area, providing accurate images over an extended period of time. On the other hand, a system that would use as reference RSS only the measurements collected during an initial calibration phase would not be able to adapt to the changes of the propagation patterns. Figures 4.4.9 (f)-(j) show how in this case the noise of the images produced by the system would quickly increase to the point of making a reliable estimate of the person's location impossible.

A drawback of using the moving average to update the reference RSS is that when the person is stationary, $\bar{r}_{l,c}(k)$ will over time approach $r_l(k)$. Thus, the link measurement $y_l(k)$ in Eq. (4.4.1) will have a very small value and the red blob indicating the position (see Figures 4.4.9 (a)-(e)) of the person will vanish in the background noise, making localization of the person difficult. To avoid the disappearing of the blob when the person is stationary, only those links that are far away (e.g. two meters) from the current position of the person can be updated. In [42], a circular gating area centered at the current location of the person was used to determine which links to update and which not. Using the method, links of the network not intersecting the gating area are recalibrated online, while the ones intersecting the gating area are not recalibrated. The method has been demonstrated to be sufficient for updating the reference RSS online without losing track of the person even though they would remain stationary for long time periods.

4.4.6 Future Work with DFL

RSS-based DFL is an emerging technology. Despite the advantages and high localization accuracy of RSS-based DFL, several open research questions remain before these systems can be utilized in real-world applications. These include solving the energy constraints imposed by the battery powered devices, resolving the networking requirements of DFL so that high localization accuracy can be

achieved, and designing algorithms that are able to track multiple targets simultaneously. The management framework for DFL [27] provides a solid foundation for future research when the networking issues and energy efficiency are addressed. In addition, preliminary work has been conducted to enable multiple target tracking [43].

4.5 Wearable Sensor System

4.5.1 Hybrid Localization System Architecture

A hybrid localization system with wearable sensors has been developed to estimate the location of rescue team members during operation and provide also some information on their physical state.

The system is based on wireless wearable sensor nodes and sensors installed on the clothing or equipment of the rescue team members. Location estimates are provided by GPS when moving outdoors, and by inertial or radio based methods when operating indoors. Physical condition monitoring is implemented by an inertial based activity recognition algorithm that is able to classify some common activities during operation, such as walking, standing still, ascending or descending stairs, and provide the general intensity level of the current activity.

Implemented system architecture is shown in Figure 4.5.1. The following operational components are included in the system:

- 3 wearable and mobile hybrid positioning platforms equipped with 2.4GHz and 868MHz radios.
- One gateway node.
- Option to use 4 base stations equipped with 2.4GHz and 868MHz radios for radio based indoor/outdoor positioning.
- A graphical user interface (GUI) for control and diagnostic purposes of the network.

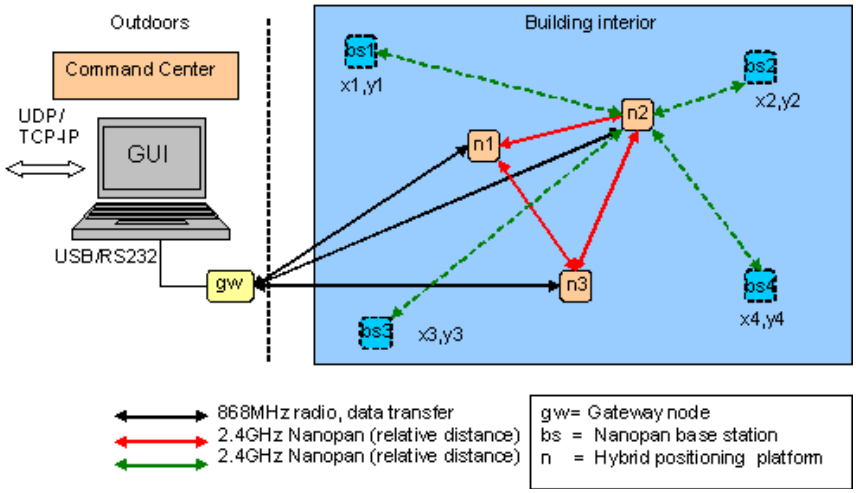

Figure 4.5.1. Hybrid localization system architecture.

The network topology in hybrid localization system is a star topology with TDMA type of data transfer. The gateway node acts as a synchronizer for the network and collects the data from the wearable hybrid positioning platforms. Relative distance between each group member is measured by the Nanopan radio.

The optional Nanopan base stations can be used for distance measurement between team members and base stations and for calculating a radio based position estimate of a team member inside (or outside) the building if the locations of the base stations are known (or definable). The graphical user interface (GUI) runs in a PC at command center and visualizes data from hybrid localization algorithms. Data interchange between external applications or user interfaces is implemented by IP socket messages (UDP or TCP-IP) via ICE interface.

4.5.2 Hybrid Positioning Platform

Hybrid positioning platform is based on an extendable and stackable general purpose sensor node architecture developed by VTT (the VTT Node). The platform consists of a microcontroller (UC) base board and a radio board connected together. Sensors are connected via digital interfaces to the platform (see Figure 4.5.2).

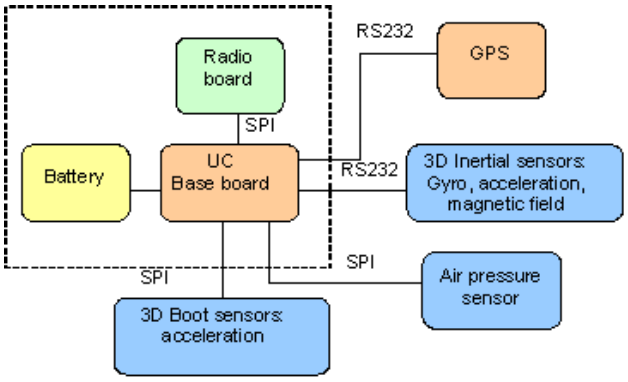

Figure 4.5.2. Hybrid positioning platform with applied sensors.

The base board together with wearable sensors performs sensor data collection, carries out some filtering tasks for sensor data, and runs inertial navigation and activity recognition algorithms. The radio board handles distance measurements between team members (and optional base stations) and wireless data transfer to the operation command center via the gateway node.

The placement of inertial navigation sensors and GPS is on the shoulders of a person and one acceleration sensor is installed on left and right foot. An air pressure sensor is placed on the back and is used to measure air temperature and altitude.

4.5.3 Wearable Sensor Node

Wearable sensor node is based on main processor board and radio expansion board connected together. VTT has developed both boards outside WISM II project. The embedded processor board (VTT Node) has been developed for general purpose sensing. The base board provides more computing power over the hybrid AVR-platform used in WISM project, and enables more possibilities on implementing algorithms in the sensor node (see Figure 4.5.3).

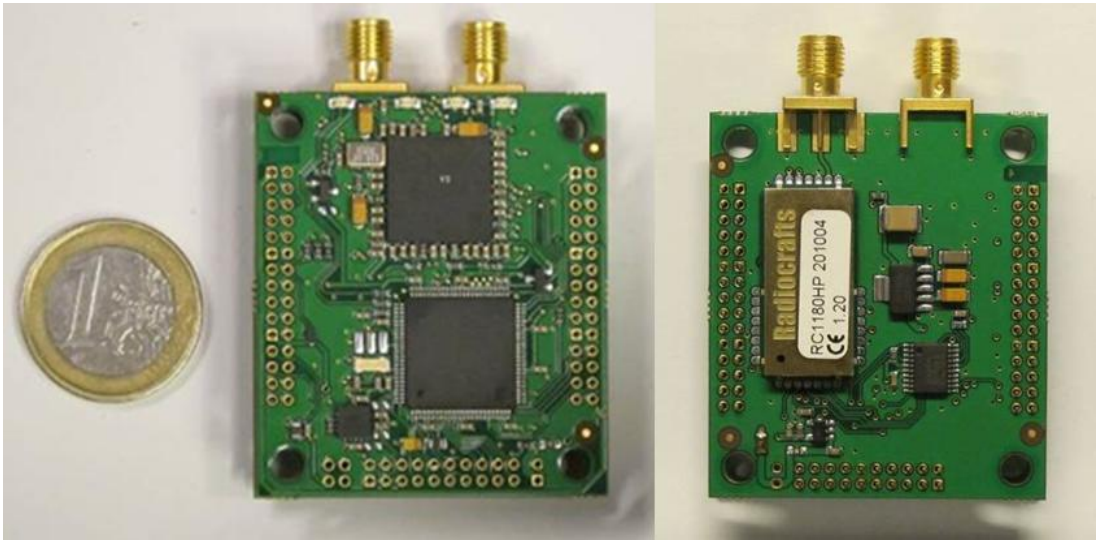

Figure 4.5.3. VTT Node base board (left) and radio board expansion (right).

The base board has the following features:

- 8 bit ATXmega up to 32 MHz and up to 1 Mgate FPGA for parallel signal processing.
- 8–16x 12 bit ADC channels and some general purpose IO lines for sensing.
- Stackable architecture with expansion modules (dual radio board, analog IO, etc.)
- Low power operation, small size, could be battery operated
- Industrial temperature range (-40-85ºC).

The WPAN board includes two different radios on the same circuit board. Both radios operate on license free ISM frequency bands.

The radio board has the following components installed:

- Nanopan 5375 radio (IEEE 802.15.4a) 2.4 GHz, maximum data rate 2 Mb/s, range 30/200m (in/outdoors); channelization features and time of flight based ranging (TOF) and 20 dB power amplifier for extended communication range.
- Long range RC1180HP-RC232 868 MHz radio; maximum data rate 78 kbit/s, up to 1 km range in line of sight conditions.

4.5.4 Applied Sensors

For inertial sensing, an M3 navigation board from Ryan Mechatronics is used (see Figure 4.5.4). M3 board includes all the sensors needed for inertial navigation, a GPS module and an onboard ARM microcontroller for measurements and data processing. M3 provides the following properties:

- 3-axis Honeywell ICHMC5843 digital Compass.
- 3-axis LIS3LV02DQ 6g accelerometer.
- 3-axis Invensense ITG-3200 gyroscope up to 1200 deg/sec.
- 32 bit LPC 1343 ARM UC (Max. 72 MHz). (collects sensor data and does pre-processing for inertial navigation algorithm).
- On board uBlox GPS module with antenna for outdoor navigation
- Freeware software for application development.
- RS232, I2C, ADC, IO and USB interfaces.

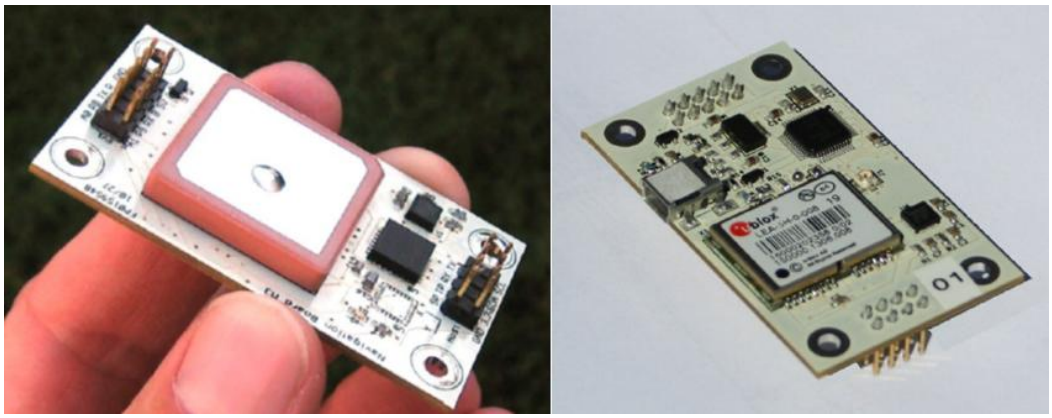

Figure 4.5.4. M3 navigation board.

The M3 module was selected because of its integrated layout. Other reasons were the sensor placement on the same circuit board with micro controller and freely available software for application development.

Both installed sensors are 3-axis SPI interfaced +-6g SCA 3100 accelerometers by VTI Technologies (Figure 4.5.5). One sensor is placed in both boots and they are used to detect steps and estimate the walked distance in order to aid the inertial navigation algorithm. Evaluation boards were used for the boot acceleration sensing in the system.

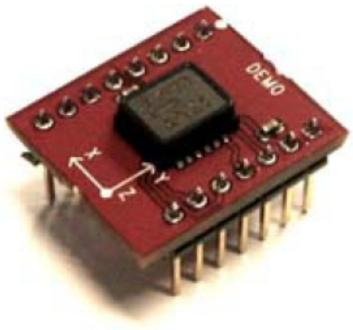

Figure 4.5.5. SCA3100 acceleration sensor.

Air pressure sensor is SCP1000 from VTI technologies.

SCP1000 has the following features:

- 30–120 kPa (ca. 10cm altitude resolution)
- Operational range -30-70 °C (temperature sensor included)

4.5.5 VTT Node Compatibility with UWASA Node

Compatibility with UWASA Node 802.15.4 radio network was considered during the project because the 802.15.4a Nanopan radio used for distance measurements operates at the same frequency band and they are not compatible with each other. To avoid collisions a simple protocol was developed. In this protocol a wearable node requests for ranging from UWASA Node network. When ranging is granted by UWASA Node network, it has halted its operation and ranging can be performed. After wearable node has indicated that ranging is complete, UWASA Node network will return to normal operation.

For transmitting ranging requests to UWASA Node network, one UWASA Node was interfaced with a wearable sensor node. It was observed in laboratory tests that implemented protocol is not highly effective and could be improved in advance if both networks are operated in near proximity. The protocol could cause delays to some timing or bandwidth sensitive parts of the UWASA Node network. Also in some cases and depending on the indoor environment the range of 802.15.4 radios could limit the receiving of the ranging requests.

4.5.6 Wearable Sensor System Installation

Figure 4.5.6 shows the wearable sensor system installation on a soldier. The M3 Navigation unit is installed on the left shoulder and the 868MHz and 2.4Ghz antennas on both shoulders. Boot sensors are installed at the sides of the boots and sensor node enclosure is placed at the back. Pictures were taken during the WISM II demonstration week (October–November 2012) in Santahamina garrison.

Figure 4.5.6. Wearable sensor system installation on a soldier.

4.5.7 Navigation Algorithms

The hybrid localization system enables estimating team member positions with separate positioning methods. Data fusion algorithms that combine position information from multiple sources for optimal positioning estimate were not developed since the project budged was reduced from the original plans of WISM II and they were left outside the work package. Hybrid positioning in implemented prototype system is defined as a combination of different indoor and outdoor navigation methods and the possibility to use the most suitable option for positioning depending on the environment. When a person moves outdoors, GPS navigation can be used. Indoor and outdoor positioning is possible by an inertial navigation algorithm or by radio positioning.

Hybrid positioning starts outside the building by utilizing the GPS signal. In this way the absolute position of the user can be established. If it is possible to take a couple of GPS-based position estimates before entering to the building, they can be utilized to calculate correction parameters for inertial navigation system.

Before entering to the building, the absolute direction of the movement can be calculated either with GPS values or with magnetometer readings, and the initial position of the user can be bound to absolute coordinates.

Activity Recognition

The activity recognition algorithm in WISM II is based on the implementation done in WISM project. Some improvements for more robust operation, faster response and reduced computational time requirements have been done in WISM II.

The algorithm is able to detect if a person stands still, lies on the floor, walks forward and descends or ascends stairs. Matlab-based offline and embedded C-language online implementation for the wearable sensor node were made. The activity recognition during the operation can be used to follow the state of the own troops inside the building.

Inertial Navigation

In the developed system the basic method for indoor navigation is the inertial navigation system. The calculation of direction of the movement is based on 3D gyro complemented with 3D accelerometer. This combination provides the means for estimating the momentary direction of the movement. Since there will be inevitable drift with gyros, also the magnetometer readings can also be used to compute absolute directions inside the building. The magnetometer must be used with care because in can be strongly affected my magnetic disturbances.

The distance of the movement is calculated by accelerometers mounted to the boots. Two time parameters are calculated for each step. The parameters are:

1) The time between the heel hitting the ground and the same foot getting up from the ground.

2) The time between consecutive steps. The best way to calculate this time difference is to use the moment when the heels hit the ground.

The range of one step, in meters, is then calculated with these two parameters, together with the length of the person and with one empirical coefficient. Adding up the ranges of separate steps then finally gives the total distance walked. Implemented inertial navigation algorithm operates together with activity recognition algorithm and calculates distance when currant activity is detected. Main navigation mode is primarily two dimensional but also limited 3D navigation is possible. When walking in stairs the altitude will be changed by fixed size of amounts during each step depending on the type of activity.

Also the 3D accelerometer, situated in the back, can be used to evaluate the distance, but the use of boot sensors is more accurate.

If possible, the position is adjusted with the GPS signal. However, this mode of hybrid positioning can be used only occasionally, e.g., if the person halts for a moment under a roof window or respective structure, which allows a line of sight required for the satellite positioning.

Radio Positioning

Two algorithms for radio positioning are available. The first one can be used only in 2D navigation. The second one can be used in 3D (or 2D) navigation depending on the navigation parameter setup. In both cases the location estimation is using base stations which are placed in pre-defined coordinates.

2D radio positioning algorithm is based on the following:

1) Measure definable number of distances to the radio positioning base stations once in a second.
2) Filter distance data. Options for filtering are average, median or minimum value.
3) Limit distance value variation in time.
4) Calculate positioning estimates. This results in 0-4 position estimates by the circle interception method.
5) Filter position estimates with average or median filter.
6) Limit positioning estimate variation in time.
7) Display estimated location coordinates.

In 3D algorithm the location estimation uses four or more base stations (4 base stations are available in the current system). The location estimation is carried out in two phases. First, an initial estimate is calculated based on four or more filtered distance measurements to base stations and then an optimal estimate is calculated iteratively using the initial estimate as an initial value for the estimated location parameters. Detailed information on the algorithm can be found in [44]. 3D algorithm was found to be functional but it requires good quality distance measurements with small variation to function properly (effective iteration and smaller positioning estimate error). We found indoor environments to cause too

much variation in measured distance values. Also requirement for successful ranging to all four base stations cannot always be guaranteed indoors.

4.5.8 Graphical User Interface and ICE

Graphical user interface for control and diagnostics purposes was created with Visual Studio 2010 and in C++ language. The interface enables local data collection from wearable nodes and visualizing the navigation and activity recognition related information. Then ICE-interface is used to integrate the wearable sensor system with the rest of the indoor situation modeling system. Via ICE all the data available in the user interface data can be interchanged with external applications or user interfaces for further processing and visualization.

4.6 Computation and Sharing of Common Operational Picture

There is the IceStorm middleware used for data management and COP server for common operational picture computation, visualization and distribution. IceStorm middleware is used to collect and log down the data from different subsystems. COP server then orders the data it needs for COP computation by using IceStorm. In addition to WNS and robot sensor measurements, this software architecture allows us to add also other sources of information to COP, if such sources are available.

The COP server encapsulates multiple functions, such as hosting relevant information, targets, information fusion as well as publishing the result. These entities are presented in Figure 4.6.1.

A command and control application is running as a front end application for the COP server, which provides a user interface for the command post operator. In addition, it hosts multiple services needed by the system, such as information sharing and operative sharing services. The produced result is the COP model (see Figure 4.6.1), which includes all information that is significant for supporting situation awareness.

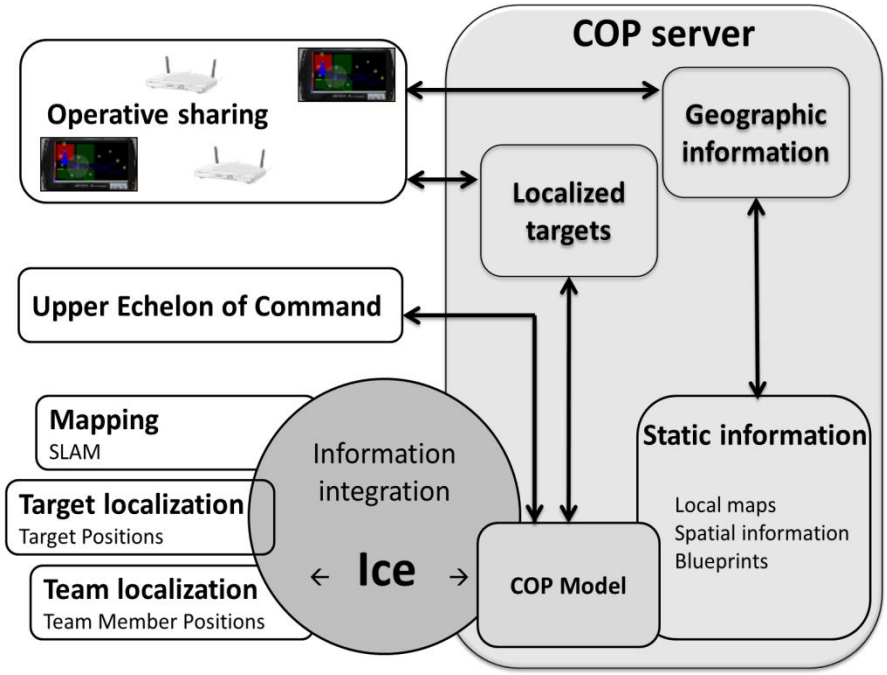

Figure 4.6.1. COP server framework.

The mobile application, shown in Figure 4.6.2, was created on Android platform. Android was chosen because it allows easy deployment on new devices using the same operating system, and makes it possible to use a wide range of COTS products. The application is designed to be as simple as possible for the user to perceive the current operational picture. Common use cases are moving the map, zooming the map, and adding a new object. Every feature is available by using only one hand, including opening the carrying pouch, where it is attached on the torso of the user.

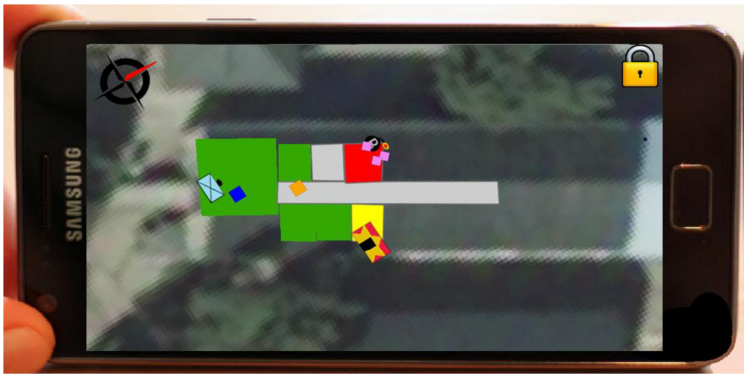

Figure 4.6.2. Handheld device graphical user interface for assisting situation awareness.

5 EXPERIMENTS

5.1 The Performance of the Device Free Localization

In the following, we present experimental results of DFL in three different indoor environments: an open indoor environment, a cluttered apartment deployment and a challenging through-wall scenario. We exploit the methods presented in Section 4.4, i.e., the fade level-based spatial and measurement models. We call this method fade level RTI (flRTI).

5.1.1 Experiment Description

The sensors used in the three experiments are Texas Instruments CC2531 USB dongles, set to transmit at the maximum power, i.e. +4.5 dBm [45]. The sensors communicate in TDMA fashion on multiple frequency channels. The IEEE 802.15.4 standard [46] specifies 16 channels within the 2.4 GHz ISM band. They are numbered from 11 through 26 and are 5 MHz apart, having a 2 MHz bandwidth.

The sequence of transmission is defined by the unique sensor's ID number. In each packet, the sensors include their ID and the most recent RSS measurements of the packets received from the other sensors of the network. If a packet is dropped, the next sensor in the schedule transmits after a back-off time, thus increasing the network's tolerance to packet drops. At the end of each communication cycle, the sensors switch synchronously to the next frequency channel found in a list pre-defined by the user. The communication protocol is explained in further detail in [42].

On average, the time interval between two consecutive transmissions is 2.9 ms. For example, a communication cycle of a network consisting of 30 sensors takes 87 ms and if four channels are used, the sampling interval on each channel is 348 ms. Due to the low latency between transmissions, the human induced changes in RSS on the different channels are correlated.

In experiment 1, shown in Figure 5.1.1 (a), 30 sensors are deployed on the perimeter of the monitored area (70 m2). The sensors are placed on podiums at a height of one meter. The sensors are programmed to communicate on channels 11, 17, 22, and 26 so as to cover the entire span of available frequencies. During the test, a person walks at constant speed along a rectangular path. The trajectory is covered multiple times to collect a sufficient number of RSS measurements. Markers

are placed inside the monitored area for the test person to follow, while a metronome is used to set a pre-defined walking pace. In this way, each collected RSS measurement can be associated to the true location of the person.

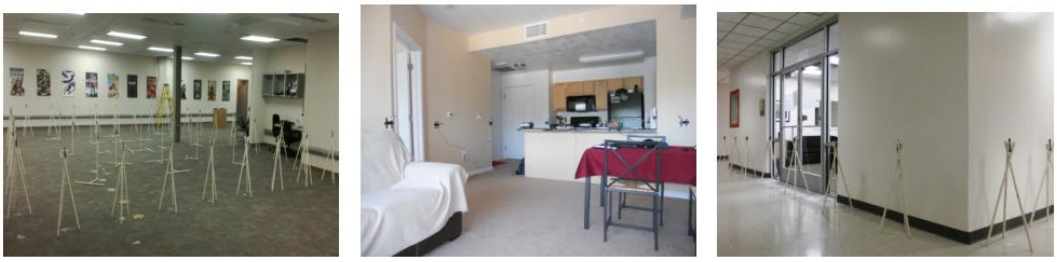

(a) Open environment (b) Apartment deployment (c) Through-wall scenario

Figure 5.1.1. The three environments used in the experiments.

In experiment 2, shown in Figure 5.1.1 (b), 33 sensors are deployed in a single-floor, single-bedroom apartment (58 m2). Most of the sensors are attached on the walls of the apartment, while a few of them are placed elsewhere, e.g., on the edge of a marble counter in the kitchen or on the side of the refrigerator. The antennas of the sensors are detached from the walls by a few centimeters to enhance the localization accuracy [20]. In the experiment, the sensors are programmed to communicate on channels 15, 20, 25, and 26 in order to avoid the interference generated by several coexisting Wi-Fi networks found in the neighboring apartments, which would increase the floor noise level [47]. As in experiment 1, a person walks along a pre-defined path at constant speed several times.

In experiment 3, shown in Figure 5.1.1 (c), 30 sensors are deployed outside the walls of the monitored lounge room (70 m2). The sensors are set on podiums as in experiment 1. Five channels (11, 15, 18, 21, and 26) are used for communication and the channels are selected approximately equidistant on the frequency scale so as to cover the entire span of available frequencies. During the experiment, the person is standing still at one of ten predefined positions, located along a rectangular perimeter so to evenly cover the entire monitored area. Experiment 3 is solely a localization experiment.

5.1.2 Estimated Image Quality

Radio tomographic imaging aims to form an image description of an object by measuring a radiating field that is modified by the object and by relating the measurements to the physical distribution of the object. The estimated distributions of the person in the through-wall experiment with three different RF tomography methods are shown in Figure 5.1.2.

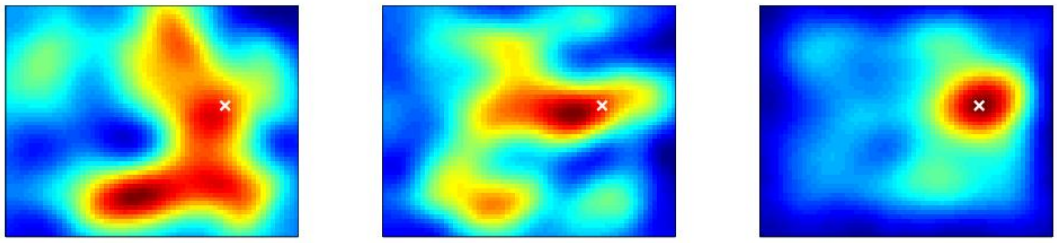

(a) Single frequency channel RTI (b) Channel diversity RTI (cdRTI) (c) Fade Level RTI (flRTI)

Figure 5.1.2. The estimated distribution of the person in the RF propagation field with three different radio tomographic imaging methods. The true location of the person is represented by the white cross in the figures.

In Figure 5.1.2 (a), attenuation of the RF signals on a single frequency channel are exploited while estimating the distribution of shadowing losses [15]. In a through-wall environment, links measuring shadowing of the person are sparse. In addition, links can be affected even far away from the link line since in this type of environments multipath propagation is common. Due to these two reasons, the performance of the system is satisfactory and as shown in Figure 5.1.2 (a), the computed image leads into a poor estimate of the person's location. In Figure 5.1.2 (b), communication on multiple frequency channels is exploited to increase the number of link measurements and methods proposed in [20] are used to estimate the image. Channel diversity increases the probability that at least one of the channels captures the human-induced shadowing and as shown, the peak of the estimated distribution is close to the location of the person. However, the dispersion of the distribution is large and there are artifacts (shadowing losses not naturally present) in the image since the method makes use of a spatial weight model relying on a fixed λ value. In Figure 5.1.2 (c), the image is estimated using flRTI. As shown, the estimated distribution coincides with the true location of the person and there are no severe artifacts in the image. The fade level-based measurement model is able to more precisely capture the human-induced RSS changes and the fade level-based spatial model is able to more accurately relate the measurements to the true location of the person.

5.1.3 Localization and Tracking

From the estimated image in Eq. (5), the position of a person can be determined by finding the voxel of the image that has the maximum value, i.e.,

$$n = \arg\max_N \hat{\boldsymbol{x}}. \tag{5.1.1}$$

Thus, the position estimate is $\hat{z} = z_n$, where z_n represents the center coordinates of voxel n. For tracking the movements of a person, we apply a Kalman filter [48] as in [49]. To quantify the accuracy of the system in the following section, the average error $\bar{e}$ is defined as the root-mean-squared error (RMSE) of the location estimates

$$\bar{e} = \sum_{k=1}^{K} \|\hat{z}(k) - z(k)\| \tag{5.1.2}$$

where K is the total number of estimates and $z(k)$ is the true location at time k.

5.1.4 System Performance

The true and estimated trajectories of the person during experiment 1 are shown in Figure 5.1.3 (a) when using flRTI. The proposed system is capable of tracking the person with an average error of $\bar{e} = 0.17$ m in the open environment. Respectively, the true and estimated trajectories of experiment 2 are shown in Figure 5.1.3 (b). The average tracking accuracy is $\bar{e} = 0.23$ m in the apartment deployment. The true and estimated positions of experiment 3 are shown in Figure 5.1.3 (c). The average localization error is $\bar{e} = 0.30$ m with flRTI. For comparison, the method proposed in [20] achieves and accuracy of $\bar{e} = 0.72$ m in the through-wall scenario as shown in Figure 5.1.3 (c). The improved performance, as a result of applying flRTI, is due to the fact that in the through-wall scenario the number of links measuring attenuation when the link line is obstructed is sparse. Furthermore, in this type of environments it is common that human-induced changes in the RSS are observed also elsewhere than on the link line, which the system in [20] is not able to capture since it uses a weighting model relying on a fixed λ.

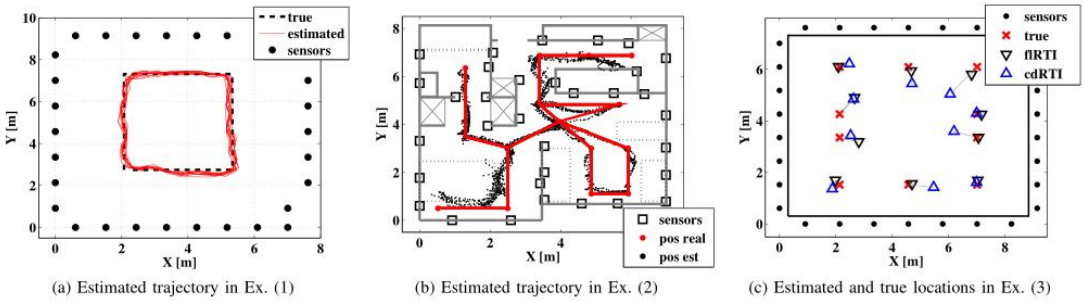

(a) Estimated trajectory in Ex. (1) (b) Estimated trajectory in Ex. (2) (c) Estimated and true locations in Ex. (3)

Figure 5.1.3. System performance in the three different environments.

5.2 Localization and Mapping by the Mobile Robot

5.2.1 Robot Self-Localization and Mapping

Simultaneous Localization and Mapping (SLAM), is a well-studied field and there are several approaches for solving it. Here, the requirements are to map an arbitrary environment in real time, and the frame-of-reference should not change during mapping. Because of this, the problem was approached using a grid-based mapping and tracking (or Maximum Likelihood SLAM) method. This approach incrementally builds an occupancy grid through two steps: 1) Tracking, which maximizes the observation likelihood given the map, and 2) mapping, which fuses the observation with the map into the pose provided by the tracking step. This approach does not employ any loop-closing mechanisms, and therefore we refer to it as mapping and tracking in order to distinguish it from a full SLAM solution.

The mapping step is a trivial occupancy update step using known pose and laser scanner data with a line model [50]. The tracking step uses a globally optimal search algorithm introduced in [51] for finding the best pose in the map. The search algorithm branches the pose space, with an objective to minimize the point distance to occupied map cells. The solution is bound by using an efficient approximation of the upper and lower bounds of the objective. The algorithm has been shown to provide robust, sub-resolution pose estimates even with very large search spaces [51] and being able to map accurately even in the presence of large loops [8]. In this use-case, the map is incrementally built, and thus the search space is relatively small. The robot mapping and tracking inside the target area is shown in Figure 5.2.1.

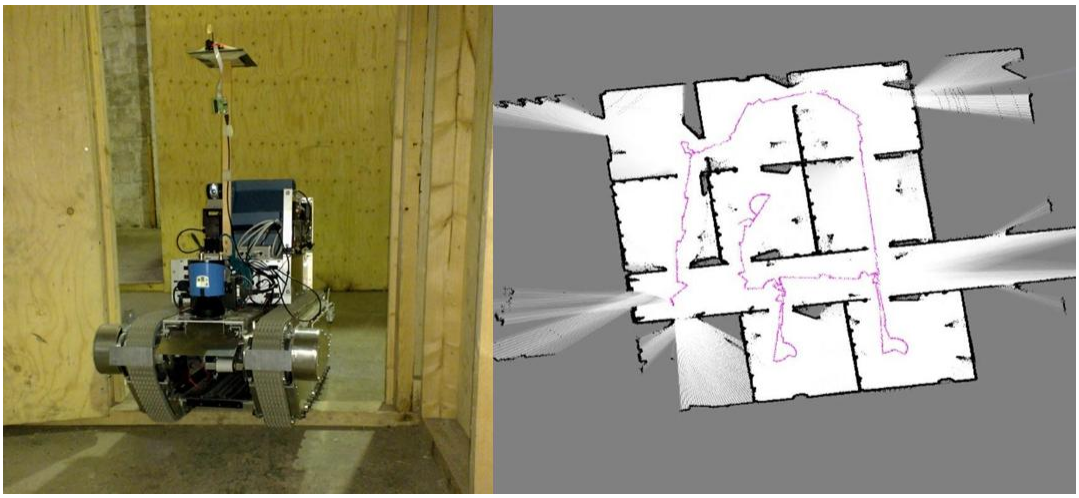

Figure 5.2.1. The robot in the test environment and an example map from the test scenario.

The rightmost part of the Figure 5.2.1. provides an example map from the test scenario. The map is built in real time by the robot and it shows an exploration through eight rooms. The map is published to the other subsystems as an image in every 10 seconds. It is then used in the command center to provide additional details about the environment structure and it is overlaid with the a priori map and global geographical information in the COP server. The map is also provided to the robot operator in order to help in keeping spatially oriented while driving the robot. The pose of the robot is published to ICEStorm continuously, for the other subsystems, specifically the robot operator and the node localization system.

5.2.2 Sensor Node Localization by using the Mobile Robot

There are many existing localization methods for WSN. Those aiming for global localization require a set of references or beacons placed in a known position. Using this position and measurements such as received signal strength (RSS) or time of arrival (ToA), the position of the node can be estimated by using different algorithms [52].

In the most challenging scenarios of the situation modeling we cannot assume the existence of preinstalled infrastructure. Such cases are, for example, emergency and rescue situations in which the area might be completely unknown and accessed for the first time. Sensor nodes must be deployed ad-hoc and usually in random and unknown positions, and there will be no possibility to install beacons to precise known locations.

In WISM II, we propose to use the robot as a mobile beacon to localize sensor nodes deployed in unknown positions. For that purpose, the robot is equipped with one of the nodes of the network. While the robot is exploring the environment, it is naturally communicating with the other nodes. At the same time, all the nodes are measuring the RSS of the received packets, and this information is sent to a central server. The robot position is known at all times (see section 5.2.1), and therefore every measurement can be associated to the robot position.

The algorithm used for localization is a maximum likelihood (ML) using radial received signal strength (RSS)-distance models. Using RSS as a primary source of information for localization has advantages and drawbacks. First, the circuitry to measure RSS is cheap and most of the radio chips on the market provide some sort of RSS indicator. On the other hand, RSS can be significantly affected by obstacles, and as a consequence, localization using RSS is known to be considerably inaccurate in cluttered environments. However, this sensitivity can be exploited to detect and track objects or persons by monitoring changes in the RSS, as we do in WISM II (see Section 4.4). Thus, the same source of

information can be used to both locate nodes and track people. In contrast to RSS-distance model based methods, the time based methods, such as ultra wide band, are less sensitive to the presence of obstacles and give more accurate position estimates [53]. However, they require expensive circuitry to measure time, and the technology is not widespread yet. Additionally, ranging using time based methods requires dedicated time slots, which can be a limiting factor for tracking [54].

The performance of the ML localization algorithm depends strongly on the ability of the model to make good predictions of the RSS. In cluttered environments the RSS can vary significantly, and thus the RSS is usually modeled as a random variable. Perhaps the most used RSS-distance model is the log-normal model, which is a normally distributed variable with a mean decaying proportionally to the logarithm of the distance, and with a variance characterizing the variability of the observed RSS [55]. It is well known by the scientific community that the decaying factor and the standard deviation depend strongly on the particular environment. What has not been studied in detail, is how much an unproper model calibration can affect the localization accuracy. This issue has special importance in WISM II project, since we cannot assume that there would be enough time for a proper calibration phase in the indoor situation modeling scenario. In a field study, where we used our robots and nodes in three different environemnts, we discovered that the local inhomogenity of the environment and the hardware differences among the nodes can influence significantly the model parameters. This, in turn, can have a strong negative effect on the localization accuracy [56]. To mitigate these effects we cannot count on having pre-calibrated models, but we have to rely on methods to simultaneously locate the nodes and calibrate the model. We also proposed to use one model for each node, which will take into account automatically the effects of the particularities of each node's hardware and local environment [56].

The problem of simultaneous node localization and model parameter estimation can also be posed by using ML or least-squares (LS) principles, leading to a nonlinear optimization problem, which can be solved using any standard nonlinear optimization techniques.

Another conceptually simple approach is a recursion consisting of 2 steps: Starting from the initial guess of the model parameters, first estimate the nodes positions. Then, using the newly estimated positions, re-estimate the model parameters, and start the cycle again. This idea has been proposed in [57] by using fixed beacons. In WISM II, we extended the same principle by using a robot as a mobile beacon and by using an individual model for each node. We also considered the use of higher order polynomials in the model to be able to take into account the deviations from the ideality of the log-normal model in inhomogenous environments.

In the developed system, a localization accuracy of 47 cm was achieved in a large uncluttered space and approximately 1 meter accuracy in a semi-open lobby and a typical office environment [58].

We carried out a set of experiments in 3 different environments: a large open basketball field, a partially obstructed hall of a building and a typicall modern office. The results are presented in Figure 5.2.2. The mean node localization error using our system was of 0.47, 1.06 and 0.97 meters respectively [58].

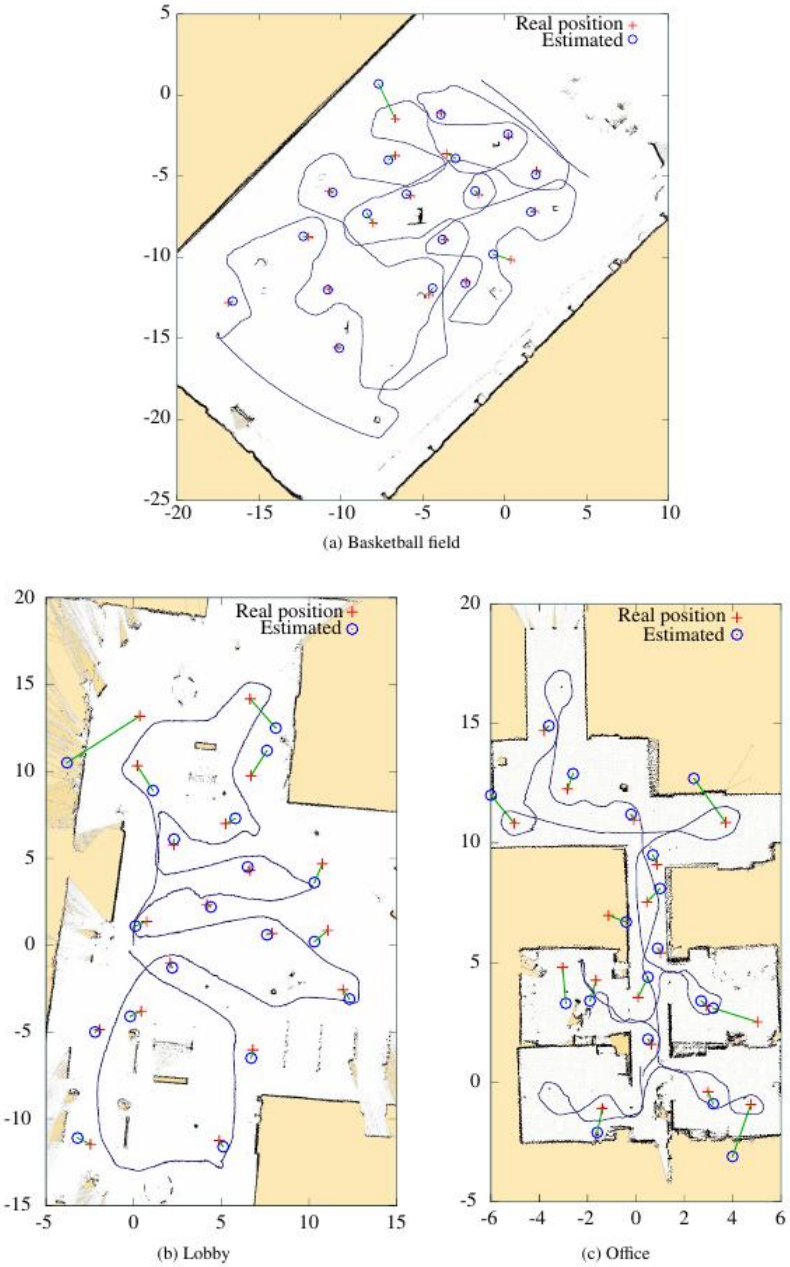

Figure 5.2.2. Localization results in three different environments by using the proposed algorithms and the robot as a mobile beacon.

5.3 Indoor Navigation by Using the Wearable Sensor System

This section presents some test results that were collected with the hybrid localization system. The data has been collected in the experiments at VTT Oulu and at Helsinki simulator in National Defence University.

5.3.1 Inertial Navigation

In Figure 5.3.1. an inertial navigation test has been performed in the office environment inside VTT Oulu building. In the experiment a loop of approximately 40 m has been walked once in the office floor. X/Y position error between start and end point was approximately 3 meters in this test. Activity recognition indicates walk by green colour.

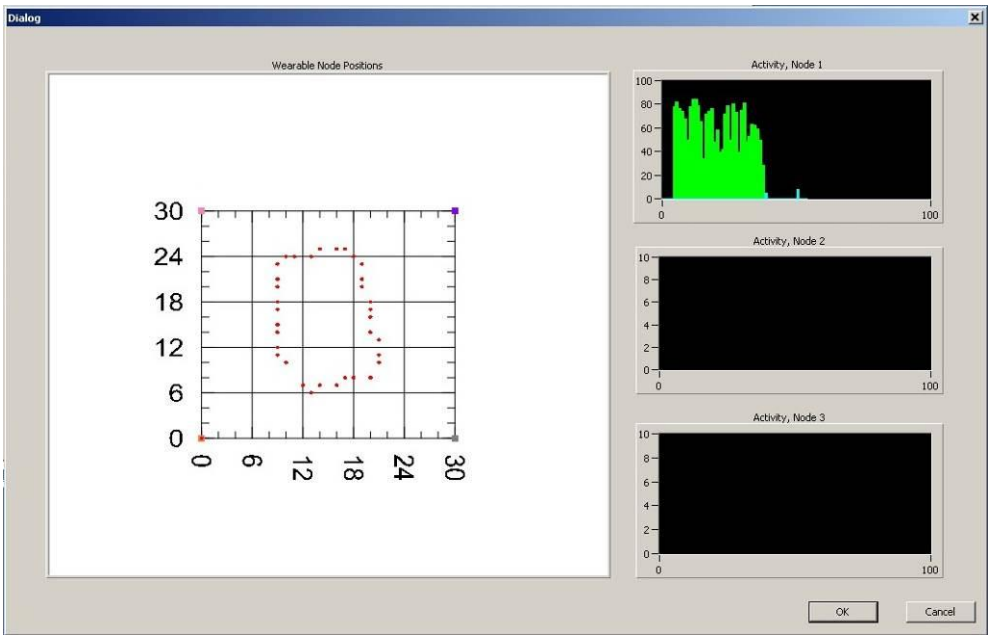

Figure 5.3.1. Inertial navigation experiment at the office environment in Oulu.

5.3.2 Activity Recognition

The experiments included a walking trip from upstairs via stairs two floors down and returning back to the starting point. Results are shown in Figure 5.3.2. there Green indicates walking on level, blue going down stairs and red rising up stairs.

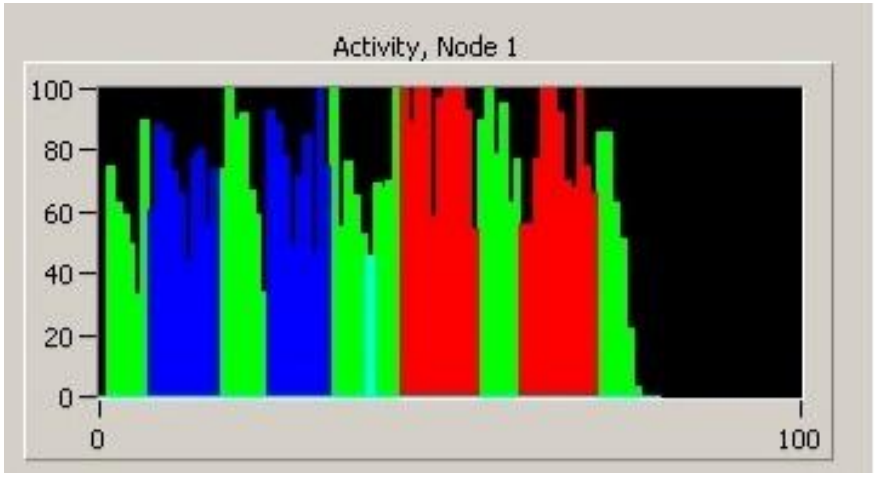

Figure 5.3.2. Intensity and the type of the current activity.

5.3.3 Radio Positioning

In Figure 5.3.3, a radio positioning test has been performed inside a room in VTT Oulu building (Innovation kitchen downstairs). 2D algorithm has been used. There were a couple of chairs and tables in the room and the size was approximately 10 x 8 m. The radio positioning base stations were installed at the corners of the room. A route was walked once inside the room in numbered order. The plotted distances present minimum value of 5 consecutive distance measurement to each base station performed once in a second. TOF position graph indicates the estimated position by the positioning algorithm. Median positioning filter and position estimate variation limiting have been used.

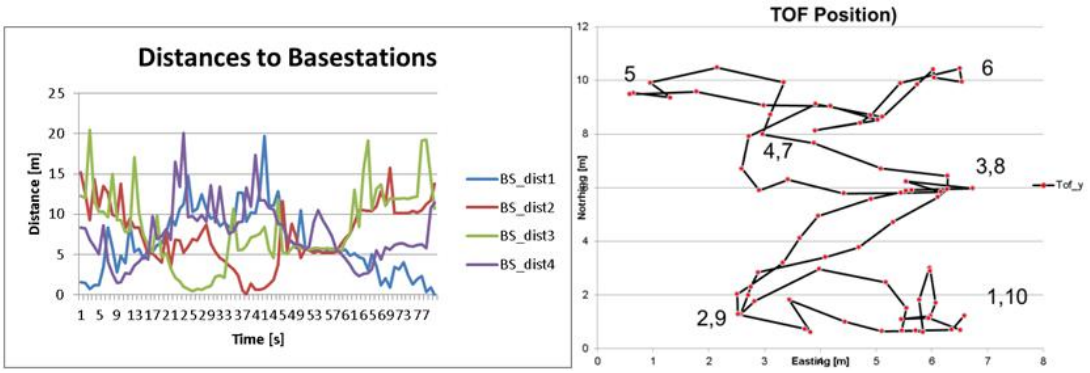

Figure 5.3.3. Indoor radio positioning test with Nanotron radios at VTT Innovation Kitchen.

In Figure 5.3.4, the radio positioning test has been performed outdoors at VTT parking area. 2D algorithm has been used. The parking area was empty during the test. A route was walked once and GPS and radio based position estimate was tracked during the walk. Simple filtering (spike removal) has been applied to the distance values. Average positioning filter has been used and no limiting has been applied to the position estimate variation. One distance measurement to each base station was performed once in a second.

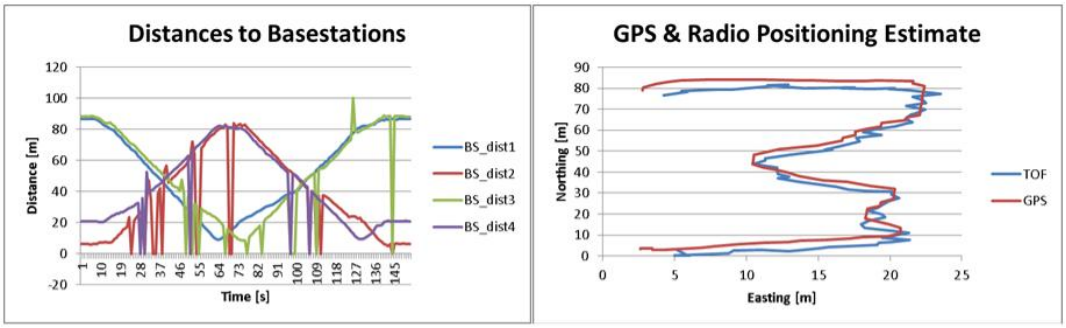

Figure 5.3.4. Outdoor positioning test with Nanotron radios.

In Figure 5.3.5, a radio positioning test has been performed in Helsinki Simulator in Santahamina. 2D algorithm has been used. The test room was approximately 8 m wide and 9 m long. Base stations for radio positioning were installed near the corners of the room. In this test a path was walked once near the walls of the room. Distances, which were utilized in the localization, were computed by selecting each time the minimum value of 5 consecutive distance measurement to each base station. TOF position graph indicates the estimated position by the positioning algorithm. Median positioning filter to limit the position estimate variation was used.

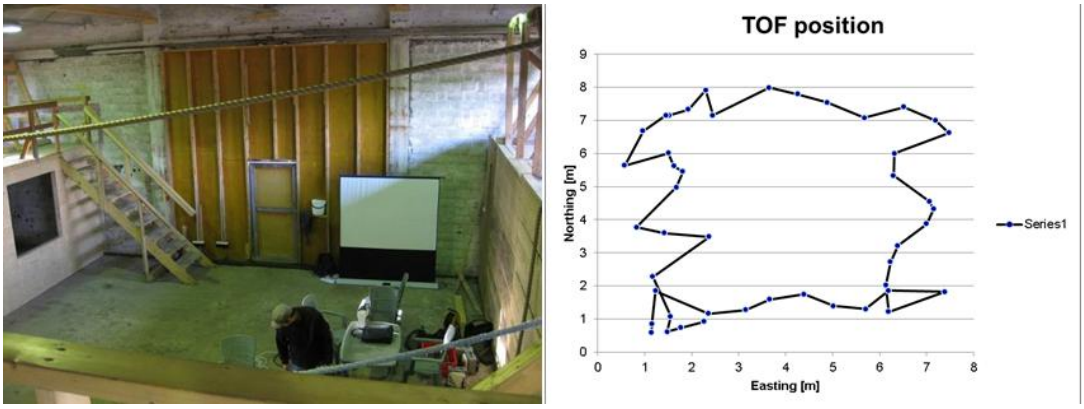

Figure 5.3.5. Radio positioning test in Santahamina.

In Figure 5.3.6., an inertial navigation test has been performed in Helsinki Simulator. In the test a corridor was walked back and forth once. Error between start and end point of was roundly 3 meters.

Figure 5.3.6. Inertial navigation test in Santahamina.

5.3.4 Indoor Navigation Summary

In WISM II, a prototype of hybrid localization system for rescue team member monitoring and positioning was developed. Implemented system provides an extendable platform to collect sensor data for different applications which require indoor navigation.

Activity recognition was found to work reasonably well among the test persons who were using the wearable sensor set. Accurate indoor navigation was found to be challenging to implement. In inertial navigation, the walked distance estimation was working quite accurately after the algorithm was calibrated for the walker. The challenge in inertial navigation was to produce accurate heading estimate and keep position and heading drift small. Since the body movement varies between constant and arbitrary during walking, the heading body angle compensation must be made in the navigation unit. In radio positioning the challenges were caused by the properties of the radio path in 2.4 GHz band (reflections, fading, multi-path) and by the limited penetration of 2.4 GHz radio signal. These phenomenas caused inaccuracy to the distance estimation, which affected on the accuracy of the positioning algorithm.

In future work the activity recognition algorithm could be developed further to detect more physical states (e.g., running, crawling, taking sidesteps). For more complete physical state monitoring, the wearable sensor system could be

extended in future with sensors that monitor the vital signs of the group member, for example, heart rate, body temperature etc. The drift minimization and correction in the inertial navigation should also be implemented. This can be done by using different data fusion algorithms that combine reference position with radio based methods or by using other technique like map matching, if building indoor map is available. Since the implemented inertial navigation also enables the detection of certain activities, the use of Inertial Measurement Units (IMU) that can be operate independently, can also be considered.

5.4 Acoustic and Visual Sensing by Deployable Sensor Nodes

5.4.1 Acoustic Sensing

Since the feature vector computation implementation to UWASA Node (see 4.3.1) was dropped from this project, we can just refer to our older results with Mica Z motes [10]. In those experiments we tested the identification by using a self-collected database of 60 individuals, 190 samples and 15 languages. The scarce resources of the sensor nodes were taken into account by setting the maximum sample rate to 8 kHz and the maximum sample length to 8 seconds. The results are presented in Figure 5.4.1. The maximum achived matching accuracy was 78%.

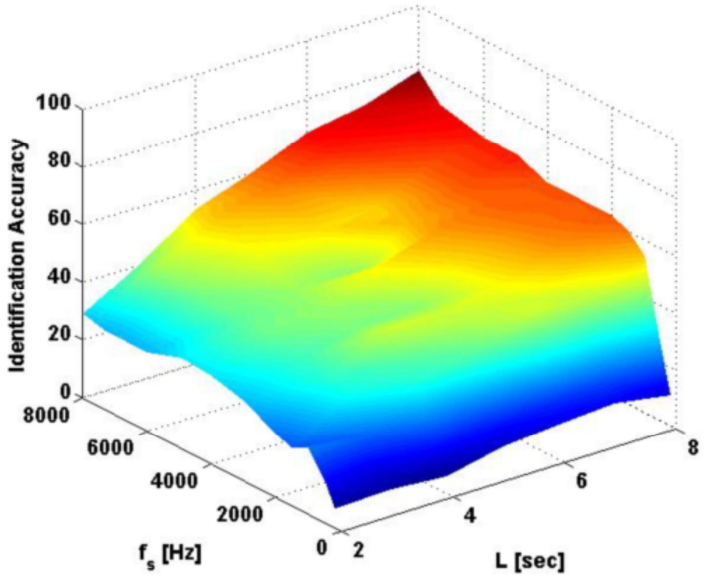

Figure 5.4.1. Speaker identicfication matching accuracy as a function of the sample length and the sample rate. The result is from older experiments [10].

In [10] we also varied the number of bins used in the discrete Fourier transform from 128 to 2048. The number of cepstral coefficients is upper limited by the number of bins such that $N_{cep} \leq N_{bins}/2$. We varied their number respectively from 10 to 1024. The speaker identification algorithm is not that sensitive for N_{bins}, but N_{cep} plays a big role. The best accuracy was reached when $N_{cep} = 100$. With smaller values the accuracy rapidly decreases. As presented in Figure 5.4.2, the accuracy slightly decreases also when $N_{cep} > 100$. This is explained by the fact the higher order mel-frequency cepstral coefficients carry less information than the lower order ones, and they tend to overlearn the spectral features of the signal [10].

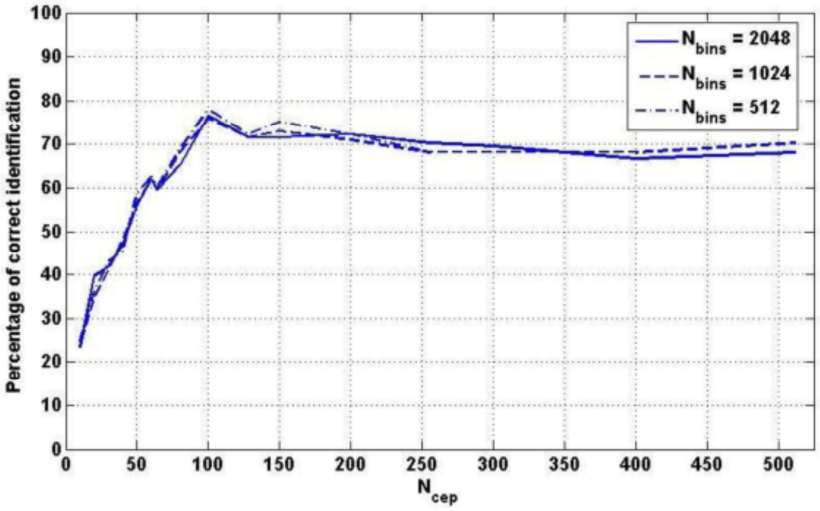

Figure 5.4.2. The effect of the N_{cep} on the algorithm accuracy [10].

During WISM II we have improved the matching accuracy by modifying the filters used in the signal processing. We have also come up with the idea that as a part of the feature vector computation implementation to UWASA Node, we can reduce the amount of data by applying the Goertzel algorithm to select such bins from DFT, which rely in the area of human speech. On the other hand, we know that this selection would reduce the richness of the data, but the effect it has to the speaker identification accuracy will be one of the research questions.

5.4.2 Visual Sensing

The CMUcam3 was implemented to UWASA Node and tested in laboratory setup [12]. Since the images usually contain much larger data than most other forms of information, image processing in wireless sensor nodes need to be limited up to a reasonable level. In addition to that, some easy computing methods should be

preferred to reduce computation efforts and lengthen battery life [59]. Following methods were introduced to achieve fast and efficient image processing.

Captured color pixels were first transformed to monochrome format before receiving the whole picture frame. This pre-processing method reduces the memory usage to quarter. While the pixel reception is still going on, the monochrome frame already starts to be built up. After this stage, a lightweight implementation of a gradient calculation followed by an edge detection algorithm is applied in order to find the edges inside the picture.

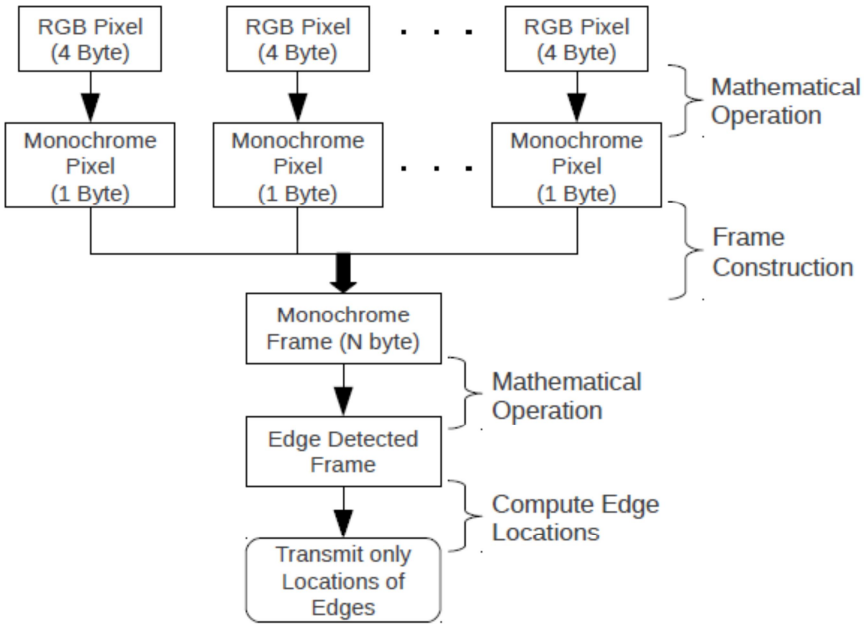

Figure 5.4.3. An example of the feature extraction with CMUcam3 implementation [12].

Figure 5.4.4 shows the different stages of some images in RGB, monochrome and gradient calculated form. As it can be noticed from the figure, the gradient calculation is able to calculate the edges not only in horizontal and vertical directions, but in circular patterns too [12, 60].

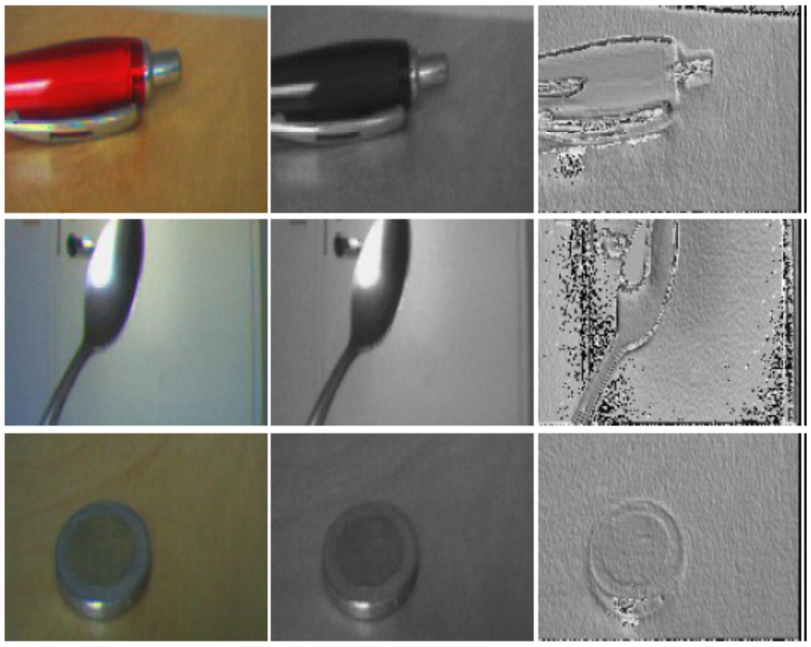

Figure 5.4.4. Original, monochrome and the gradient of some images taken by CMUcam3 [12].

After computing the gradient images, the edge detection algorithm extracts the pixels that represent the edges of the object. Basically it marks the pixels having a derivation of more than a defined filter value. Some examples are represented in the Figure 5.4.5.

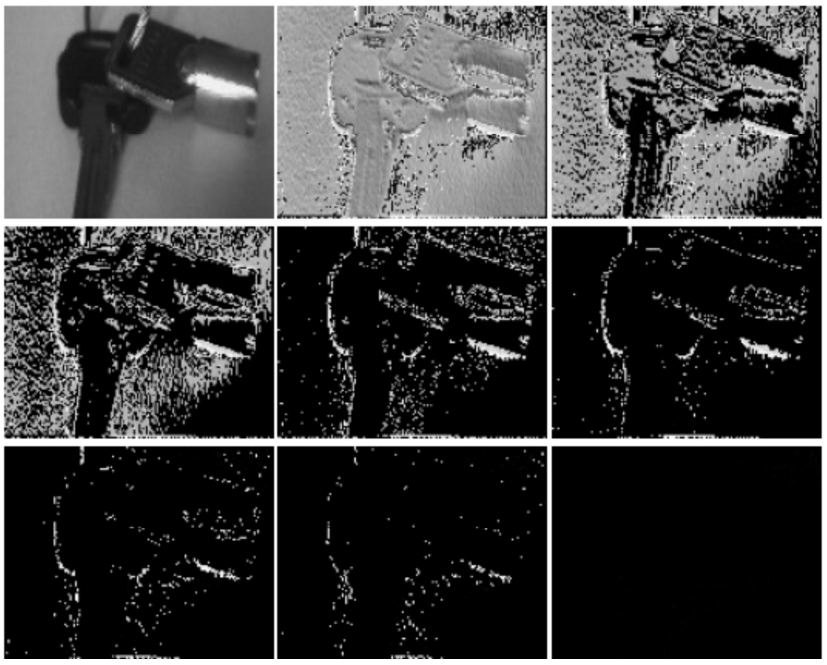

Figure 5.4.5. Original, monochrome and edge detected images [12].

In this example it can be seen that the edges of the object are calculated and their patterns are marked as white dots. By only transmitting the horizontal and vertical indexes of these pixels, it is possible to have information about the objects while greatly reducing the required amount of data to transmit. The Figure 5.4.6 shows the amount of data required to transmit the images in Figure 5.4.5.

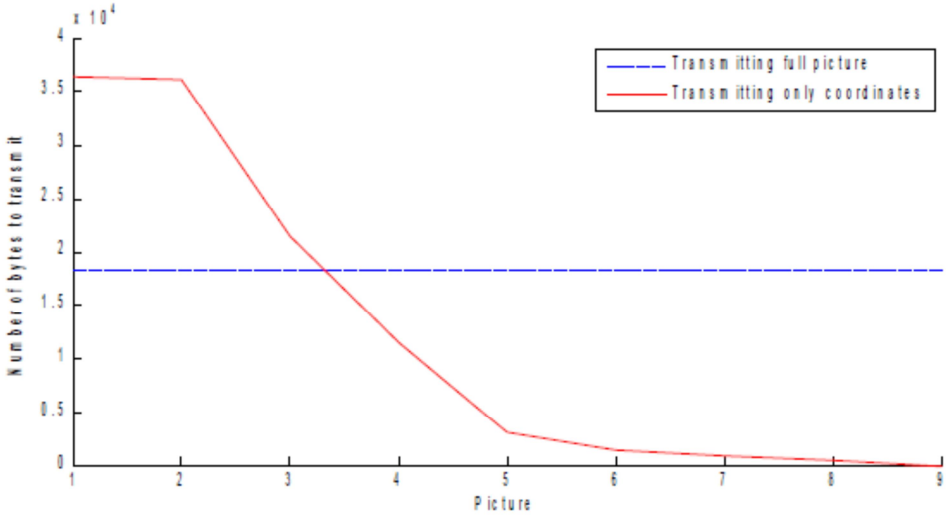

Figure 5.4.6. The amount of data required to transmit the images in Figure 5.4.5 [12].

Comparing the plot and the edge detected images above it can be concluded that transmitting only the pixel coordinates for the pictures from number 5 to 7 would provide well enough information about what these objects are. Since the first three pictures have more white pixels than the black pixels, it is not beneficial to choose coordinate transmission. In that case transmitting only the black pixel coordinates would inverse the situation and still provide great benefit in terms of network traffic.

In future, the edge detection method demonstrated in here can be developed further into contour detection, then into image segmentation, and finally into object identification.

5.5 Common Operational Picture

The demonstration setup contains a means for attaching the mobile devices to the soldier's equipment. Two options studied were attachment to the left hand (for a right-handed user) and to the upper left torso, using a specific pouch. The first impression was that the hand attachment was better, but the torso attachment

proved more reliable. The device is vulnerable when used in the hand, consuming more of the user's energy and also possibly preventing other activities during battle. The torso attachment is slightly more difficult to reach, but, on the other hand, there the device is well protected and unobtrusive. After some training, the soldiers got used to carrying and using the device attached to the torso. Later the GUI device will probably be developed to fit to this attachment more effectively. The soldiers also used glows, specially designed for tactical use with touch screen capability [61].

The users gave good feedback about the usability of the mobile devices and also on the speed of the system. More tests are needed to evaluate how well the GUI meets the needs of the users in a stressful situation. In this experiment, there was of course no extensive tiring phase (1–2 days of battle) beforehand. A test that incorporated sudden unexpected events and still forced the soldier to use the device would provide crucial information about use under the conditions of great stress [61].

During the tests, we also filmed a short movie (Finnish Combat Camera Team), which explains the operational concept of the developed system [62].

6 INTERNATIONAL COOPERATION

6.1 University of Utah

During WISM II project we started an active co-operation with Professor Neal Patwari in the University of Utah. One of the focus areas of Prof. Patwari's Sensing and Processing Across Networks (SPAN) Lab. is radio tomography, which has also been researched in this project in the context of device free localization. After completing his Ph.D. in the Department of Automation and Systems Technology of Aalto University at the end of 2011, Maurizio Bocca joined to Prof. Patwari's group as a Postdoc Researcher. Researher Ossi Kaltiokallio from Aalto University spent six months as a Visiting Researcher in prof. Patwari's group from February to July 2012. During this time several joint publications were produced [20, 32, 41-43] and the research cooperation continues.

Professor Patwari visited as a keynote speaker in Aalto University Workshop on Wireless Sensor Systems on 11th or December, 2012.

6.2 ARO Center of Excellence in Battlefield Communications

We have a long-term cooperation with Professor Dhadesugoor R. Vaman and the ARO Center of Excellence in Battlefield Communications that he directs [63]. The center is headquartered at Prairie View A&M University, which belongs to Texas A&M University System and locates near Houston.

A couple of short term visits between Houston and Finland were made during the WISM II project. On 25.-26.4.2012, professor Vaman visited as a speaker in the Workshop on Wireless Communication and Applications (WoWCA2012) in the University of Vaasa. During his visit it was also agreed that certain parts of the indoor situation modeling system developed in WISM II can be duplicated to Prairie View A&M University such that we can do parallel research and system development in the future. On February 2013, Researcher Jussi Timonen from National Defence University spent two weeks in Prairie View with Professor Vaman's group. He brought the indoor situation modeling system demonstrated on November 2012 with him and worked with the system with Prof. Vaman's group. After Jussi Timonen's visit, Senior Researcher Reino Virrankoski from the University of Vaasa spent two weeks in Professor Vaman's group. During his visit a joint seminar and a joint project proposal visit to DARPA were planned.

A joint seminar about urban situational awareness with sensors and cyber security took place at the Center of Excellence in Battlefield Communications in Prairie View on 28th of February 2013. Seminar presenters from WISM II project consortium side were Professors Heikki Koivo and Riku Jäntti from Aalto University, Professor Jouko Vankka from National Defence University and Senior Researcher Reino Virrankoski from the University of Vaasa.

6.3 DARPA

After the seminar and discussions in Prairie View, Professor Dhadesugoor Vaman from ARO Center of Excellence in Battlefield Communications, Professors Heikki Koivo and Riku Jäntti from Aalto University, Professor Jouko Vankka from National Defense University and Senior Researcher Reino Virrankoski from the University of Vaasa visited Defense Advanced Research Projects Agency (DARPA) on 1st of March, 2013. In DARPA they had a discussion about the proposed project idea (Urban Situational Awareness with Sensors) with Program Director Mark Rich. Before the meeting in DARPA the Finnish participants visited Finnish Embassy in Washington DC, and had a discussion with Assistant Military Attachés Markku Viitasaari and Kim Juhala. Juhala also joined to DARPA-visit. Based on the discussions a white paper about the proposed project has been prepared.

7 CONCLUSIONS

In this project we developed new algorithms for device free localization, for indoor navigation, for indoor space mapping, for image processing in sensor nodes, for data management and for the computation, visualization and distribution of the common operational picture (COP). These algorithms were first tested in laboratory environment and finally in field conditions as a context of the demonstration at the urban warfare training site (so-called Helsinki Simulator) in National Defence University. By utilizing these algorithms we made a fully integrated wireless sensor system, which produces a real-time situation model of the building interior [1].

During the project there were three seminars which were strongly contributed by WISM II; Workshop on Wireless Communication and Applications in the University of Vaasa on April 25th-26th, 2013; Aalto University Workshop on Wireless Sensor Systems on December 11th, 2012 and Seminar on Urban Situational Awareness with Sensors & Cyber Security in the ARO Center of Excellence in Battlefield Communications in Prairie View A&M University on February 28th, 2013. The final demonstration was at National Defense University on November 1st, 2012.

International cooperation has been active especially with the USA as explained in Chapter 6, but also EU programs and the research interests of the European Defence Agency (EDA) have been followed.

The project had connections to wireless automation research which is done by the same consortium. The software and hardware architecture of UWASA Node was originally made in Tekes-funded project Generic Sensor Network Architecture for Wireless Automation (GENSEN) on 2009-2010 [2] and then further developed in project Reliable and Real Time Wireless Automation (RIWA) on 2011-2013. The joint use and compatibility of UWASA Node and VTT Node is also considered in RIWA. In WISM II, the protocol software has been modified such that it fills the requirements of the indoor monitoring system.

There were six companies who participated to WISM II project. After the project, five of them have provided ideas how to integrate the indoor situation modeling system properties developed in WISM II into their products. There are also 2-3 other companies who have indicated their preliminary interest to participate to this research in the future because they see that it would support their product development. Even though the system implementations and demonstrations in WISM and WISM II projects have been still prototyping and proofs of concepts,

the developed system seems to have reached such a level that our next research project in this field can be company driven.

In the future work we will develop further the data fusion and collaborative networking so that the different subsystems of the developed indoor situation modeling system would better support each other during the operation. Especially the location information can be improved via collaborative networking. In addition to network information, we will also utilize digital building maps in such cases when they are available. The communication security and system fault tolerance can be increased, if more computation would be done in a distributed or locally centralized manner in the network. Indoor situation modeling system integration to other parts of the tactical communication system via long distance link will also be considered.

REFERENCES

[1] Björkbom, M., Timonen, J., Yusein, A., Kaltiokallio, O., Myrsky, M., Saarinen, J., Vallet, J., Korkalainen, M., Cuhac, C., Koivo, H., Jäntti, R., Virrankoski, R. and Vankka, J., *Localization Services for Online Common Operational Picture and Situation Awareness*, accepted to IEEE Access, 2013.

[2] Virrankoski, R. (Ed.), *Generic Sensor Network Architecture for Wireless Automation (GENSEN)*, Proceedings of the University of Vaasa, Reports 174, Vaasa 2012.

[3] Timonen, J., *Distributed information system for tactical network*, 3rd Workshop on Wireless Communication and Applications (WoWCA2012), Vaasa, Finland, 2012.

[4] Timonen, J., *A Dynamic Tactical Command System Operating with an Ad Hoc Network*, Master of Science in Technology Thesis, Master's Thesis, University of Turku, 2011.

[5] Matusiak, M., Paanajärvi, J., Appelqvist, p., Elomaa, M., Ylikorpi, T., Halme A. and Vainio, A., *Novel Marsupial Robot Society: Towards Long-Term Autonomy*, in the Proceedings of the 9th International Symposium on Distributed Autonomous Robotic Systems (DARS 2008), Tsukuba Japan, November 17-19, 2008.

[6] Saarinen, J., Maula, A., Nissinen, R., Kukkonen, H., Suomela, J. and Halme, A., *GIMnet - Infrastructure for distributed control of Generic Intelligent Machines*, in the Proceedings of the 13th IASTED International Conference on Robotics and Applications Telematics, 2007.

[7] Maula, A., Myrsky, M. and Saarinen, J., *GIMnet 2.0-Enhanced Communication Framework for Distributed Control of Generic Intelligent Machines*, in the Proceedings of the 1st IFAC Conference on Embedded Systems, Computational Intelligence and Telematics in Control, Würzburg, Germany, 2012.

[8] Myrsky, M., Maula, A., Saarinen, J. and Kankkunen, I., *Teleoperation Tests for Large-Scale Indoor Information Acquisition*, in the Proceedings of the 1st IFAC Conference on Embedded Systems, Computational Intelligence and Telematics in Control, Würzburg, Saksa, 2012.

[9] Yigitler, H., Virrankoski, R. and Elmusrati, M. S., *Stackable Wirless Sensor and Actuator Network Platform for Wireless Automation: the UWASA Node*, Aalto University Workshop on Wireless Sensor Systems, November 19th, 2010, Espoo, Finland.

[10] M. Bocca, R. Virrankoski and H. N. Koivo, *Text and Language Independent Speaker Indentification by Using Short-Time Low Quality Signals*, Workshop on Wireless Communication and Applications (WoWCA 2008), April 2, 2008, Vaasa, Finland.

[11] Bocca, M. and Koivo, H., *Real-time text and language independent speaker identification with a reconfigurable wireless network of acoustic sensors*, Proceedings of the 2008 IEEE International Confer-

ence on Technologies for Homeland Security (HST 2008), Waltham, Massachusetts, USA. 12–13 May 2008.

[12] Cuhac, C., *Camera Integration to Wireless Sensor Node*, Master's Thesis, University of Vaasa, Department of Computer Science, Communications and Systems Engineering Group, 2011.

[13] CMUcam, *http://cmucam.org*

[14] N. Patwari and J. Wilson, *RF sensor networks for device-free localization and tracking*, Proceedings of the IEEE, vol. 98, no. 11, pp. 1961–1973, Nov. 2010.

[15] J. Wilson and N. Patwari, *Radio Tomographic Imaging with Wireless Networks*, IEEE Transactions on Mobile Computing, vol. 9, no. 5, pp. 60 621–632, May 2010.

[16] A. F. Molisch, *Wireless Communications*, Wiley – IEEE, 2nd ed. Wiley, 2010.

[17] H. Hashemi, *The Indoor Radio Propagation Channel*, Proceedings of the IEEE, vol. 11, no. 7, pp. 967–978, 1993.

[18] C. Chang and A. Sahai, *Object tracking in a 2D UWB sensor network*, in 38th Asilomar Conference on Signals, Systems and Computers, vol. 1, Nov. 2004, pp. 1252–1256.

[19] J. Wilson and N. Patwari, *See-Through Walls: Motion Tracking Using Variance-Based Radio Tomography Networks*, IEEE Transactions on Mobile Computing, vol. 10, no. 5, pp. 612–621, May 2011.

[20] O. Kaltiokallio, M. Bocca, and N. Patwari, *Enhancing the accuracy of radio tomographic imaging using channel diversity*, in 9th IEEE International Conference on Mobile Ad hoc and Sensor Systems, October 2012.

[21] G. Zhou, T. He, S. Krishnamurthy, and J. A. Stankovic, *Impact of radio irregularity on wireless sensor networks*, in Proceedings of the 2nd international conference on Mobile systems, applications, and services - MobiSYS '04. New York, New York, USA: ACM Press, Jun. 2004, pp. 125–138.

[22] L. B. Ruiz, I. G. Siqueira, L. B. e. Oliveira, H. C. Wong, J. M. S Nogueira, and A. A. F. Loureiro, *Fault management in event-driven wireless sensor networks*, in Proceedings of the 7th ACM international symposium on Modeling, analysis and simulation of wireless and mobile systems - MSWiM '04. New York, New York, USA: ACM Press, Oct. 2004, pp. 149–156.

[23] M. Ceriotti, L. Mottola, G. P. Picco, A. L. Murphy, S. Guna, M. Corra, M. Pozzi, D. Zonta, and P. Zanon, *Monitoring heritage buildings with wireless sensor networks: The Torre Aquila deployment*, in Proceedings of the 2009 International Conference on Information Processing in Sensor Networks, pp. 277–288, Apr. 2009.

[24] H. Mukhtar, K. Kang-Myo, S. Chaudhry, A. Akbar, K. Ki-Hyung, and S.-W. Yoo, LNMP- *Management architecture for IPv6 based low-power wireless Personal Area Networks (6LoWPAN)*, Network Operations and Management Symposium, NOMS 2008, pp. 417–424.

[25] H. Choi, N. Kim, and H. Cha, *6LoWPAN-SNMP: Simple Network Management Protocol for 6LoWPAN*, in 2009 11th IEEE International Conference on High Performance Computing and Communications, 2009, pp. 305–313.

[26] S. A. Chaudhry, G. Boyle, W. Song, and C. Sreenan, *EMP: A Network Management Protocol for IP-based Wireless Sensor Networks*, in 2010 International Conference on Wireless and Ubiquitous Systems, Oct. 2010, pp. 1–6.

[27] H. Yigitler, O. Kaltiokallio, and R. Jäntti, *A management framework for device-free localization*, IEEE International Conference on Neural Networks (IJCNN 2013), August 2013.

[28] P. Agrawal and N. Patwari, *Correlated link shadow fading in multi-hop wireless networks*, IEEE Transactions on Wireless Communications, vol. 8, no. 8, pp. 4024–4036, Aug. 2009.

[29] A. Kak and M. Slaney, *Principles of computerized tomographic imaging*, New York: IEEE, 1988.

[30] N. Patwari and P. Agrawal, *Effects of correlated shadowing: Connectivity, localization, and RF tomography*, in IEEE/ACM Int'l Conf. on Information Processing in Sensor Networks, April 2008.

[31] M. A. Kanso and M. G. Rabbat, *Compressed RF tomography for wireless sensor networks: Centralized and decentralized approaches*, in 5th IEEE Intl. Conf. on Distributed Computing in Sensor Systems (DCOSS-09), Marina Del Rey, CA, June 2009.

[32] O. Kaltiokallio, M. Bocca, and N. Patwari, *Follow @grandma: long-term device-free localization for residential monitoring*, in 7th IEEE International Workshop on Practical Issues in Building Sensor Network Applications, October 25, 2012.

[33] A. F. Molisch, *Wireless Communications*, (Wiley – IEEE), 2nd ed. Wiley, 2010.

[34] T. S. Rappaport, *Wireless Communications: Principles and Practice*, New Jersey: Prentice-Hall Inc., 1996.

[35] J. G. Proakis and M. Salehi, *Digital Communications*, 5th ed. New York, NY: McGraw-Hill, 2008.

[36] G. Tolle and D. Culler, *Design of an application-cooperative management system for wireless sensor networks*, Second European Workshop on Wireless Sensor Networks (EWSN), 2005.

[37] X. Chen, A. Edelstein, Y. Li, M. Coates, M. Rabbat, and M. Aidong, *Sequential monte carlo for simultaneous passive device-free tracking and sensor localization using received signal strength measurements*, in ACM/IEEE Information Processing in Sensor Networks (IPSN), April 2011.

[38] J. Wilson and N. Patwari, *A fade-level skew-laplace signal strength model for device-free localization with wireless networks*, IEEE Transactions on Mobile Computing, vol. 11, no. 6, pp. 947–958, 2012.

[39] J. C. Liberti and T. S. Rappaport, *A geometrically based model for line-of-sight multipath radio channels*, in IEEE 46th Vehicular Technology Conference, vol. 2, 1996, pp. 844–848.

[40] O. Nørklit and J. B. Andersen, *Diffuse channel model and experimental results for array antennas in mobile environments*, IEEE Trans. Antennas & Propagation, vol. 46, no. 6, pp. 834–840, June 1998.

[41] O. Kaltiokallio, M. Bocca, and N. Patwari, *A Multi-Scale Spatial Model for RSS-based Device-Free Localization*, arXiv preprint arXiv: 1302.5914, 2013.

[42] M. Bocca, O. Kaltiokallio, and N. Patwari, *Radio tomographic imaging for ambient assisted living*, in Evaluating AAL Systems Through Competitive Benchmarking, ser. Communications in Computer and Information Science, S. Chessa and S. Knauth, Eds. Springer Berlin Heidelberg, 2013, vol. 362, pp. 108–130.

[43] M. Bocca, O. Kaltiokallio, N. Patwari, and S. Venkatasubramanian, *Multiple Target Tracking with RF Sensor Networks*, Feb. 2013. [Online]. Available: http://arxiv.org/abs/1302.4720.

[44] Heikkilä T., Rehu J., Korkalainen M., Määttä K. and Pentikainen V., *Location aware multihop Wireless Sensor Network,* ICUMT 2009, St. Petersburg, Russia, 2009.

[45] Texas Instruments, *A USB-enabled system-on-chip solution for 2.4 GHz IEEE 802.15.4 and ZigBee applications*, [Online]. Available: http://www.ti.com/lit/ds/symlink/cc2531.pdf.

[46] *IEEE 802.15.4 standard technical specs*, [Online]. Available: http://www.ieee802.org/15/pub/TG4Expert.html.

[47] K. Srinivasan, P. Dutta, A. Tavakoli, and P. Levis, *Understanding the causes of packet delivery success and failure in dense wireless sensor networks*, in Proceedings of the 4th international conference on Embedded networked sensor systems (SenSys '06), 2006, pp. 419–420.

[48] Y. Bar-Shalom, X. Rong Li, and T. Kirubarajan, *Estimation with Applications to Tracking and Navigation*, John Wiley & Sons, 2001.

[49] O. Kaltiokallio and M. Bocca, *Real-time intrusion detection and tracking in indoor environment through distributed rssi processing*, in 2011 IEEE 17th Intl. Conf. Embedded and Real-Time Computing Systems and Applications (RTCSA), August 2011.

[50] Moravec, Hans P., *Sensor fusion in certainty grids for mobile robots*, AI magazine 9.2 (1988): 61.

[51] Saarinen, J., Paanajärvi, J. and Forsman, P., *Best-first branch and bound search method for map based localization,* in the Proceedings of IEEE/RJS International Conference on Intelligent Robots and Systems, San Francisco, Sep 25-30, 2011.

[52] Seco, F.; Jimenez, A. R.; Prieto, C.; Roa, J. & Koutsou, K., *A survey of mathematical methods for indoor localization,* in the Proceedings of IEEE Intelligent Signal Processing WISP 2009.

[53] Patwari N., Hero, I., Perkins, M., Correal, N. and O'Dea, R., *Relative location estimation in wireless sensor networks*, IEEE Transactions of Signal Processing, vol. 51, no. 8, pp. 2137–2148, Aug. 2003.

[54] Garcia, G. E., Muppirisetty, L. S. and Wymeersch, H., *On the Trade-off Between Accuracy and Delay in Cooperative UWB Navigation*, in the Proceedings of IEEE Wireless Communications and Networking Conference (WCNC), April 2013.

[55] Seidel, S. and Rappaport, T., *914 MHz path loss prediction models for indoor wireless communications in multifloored buildings*, IEEE Transactions of Antennas and Propagation, vol. 40, no. 2, pp. 207–217, Feb. 1992.

[56] J. Vallet, O. Kaltiokallio, J. Saarinen, M. Myrsky, and M. Bocca, *On the Sensitivity of RSS Based Localization Using the Log-Normal model: An Empirical Study*, 10th Workshop on Positioning, Navigation and Communication (WPNC 2013), March 20–21, 2013.

[57] Zemek, R., Anzai, D., Hara, S., Yanagihara, K. and Kitayama, K., *RSSI-based Localization without a Prior Knowledge of Channel Model Parameters*, in the International Journal of Wireless Information Networks, 2008.

[58] Vallet, J., Kaltiokallio, O., Myrsky, M., Saarinen, J. and Bocca, M., *Simultaneous RSS-based Localization and Model Calibration in Wireless Networks With a Mobile Robot*, International Workshop on Cooperative Robots and Sensor Networks (RoboSense 2012), August 27-29, 2012, Niagara Falls, Canada.

[59] Çuhac, C., Hüseyin, Y., Virrankoski, R. and Elmusrati, M., *Camera Integration to Wireless Sensor Node*, Aalto University Workshop on Wireless Sensor Systems, 2010.

[60] Bradski, G. & Kaehler, A., *Learning OpenCV*, 1st Ed. California etc.: O'Reilly Media Inc., 2008.

[61] Timonen, J. and Vankka, J., *Enhancing situational awareness by means of visualization and information integration of sensor networks*, Proc. SPIE 8756, Baltimore, USA, 2013.

[62] Finnish Combat Camera Team, "WISM II–project," 7 March 2013, *http://www.youtube.com/watch?v=9v1fFIHRWGE*, 5 April 2013.

[63] ARO Center of Excellence in Battlefield Communications, *http://cebcom.pvamu.edu/*.